Naval Research Laboratory
Washington, DC 20375-5320

NRL/7220/MR—2023/1

Analytical Formulations for Foam Emissivity Modeling and their Numerical Implementations

MAGDALENA D. ANGUELOVA

Remote Sensing Physics Branch
Remote Sensing Division

January 31, 2023

REPORT DOCUMENTATION PAGE

Form Approved
OMB No. 0704-0188

1. REPORT DATE *(DD-MM-YYYY)*	**2. REPORT TYPE**	**3. DATES COVERED** *(From - To)*
31-01-2023	NRL Memorandum Report	11/22/2019 – 10/19/2023

4. TITLE AND SUBTITLE

Analytical Formulations for Foam Emissivity Modeling and their Numerical Implementations

5a. CONTRACT NUMBER

5b. GRANT NUMBER

5c. PROGRAM ELEMENT NUMBER

6. AUTHOR(S)

Magdalena D. Anguelova

5d. PROJECT NUMBER

5e. TASK NUMBER

5f. WORK UNIT NUMBER
1U95

7. PERFORMING ORGANIZATION NAME(S) AND ADDRESS(ES)

Naval Research Laboratory
4555 Overlook Avenue, SW
Washington, DC 20375-5320

8. PERFORMING ORGANIZATION REPORT NUMBER

NRL/7220/MR--2023/1

9. SPONSORING / MONITORING AGENCY NAME(S) AND ADDRESS(ES)

Naval Research Laboratory
4555 Overlook Avenue, SW
Washington, DC 20375-5320

10. SPONSOR / MONITOR'S ACRONYM(S)

NRL Base 6.1

11. SPONSOR / MONITOR'S REPORT NUMBER(S)

12. DISTRIBUTION / AVAILABILITY STATEMENT

DISTRIBUTION STATEMENT A: Approved for public release; distribution is unlimited.

13. SUPPLEMENTARY NOTES

14. ABSTRACT

This report documents the work done on the sea foam emissivity as a part of the work done by an international science team on developing a radiative transfer model of reference quality for the ocean surface emissivity from L band to infrared frequencies. The focus here is on frequencies from 1 to 89 GHz. The theoretical formulation of the foam emissivity is described in details. Two numerical implementations are compared and their differences quantified.

15. SUBJECT TERMS

Passive remote sensing; Radiative transfer model; Ocean surface emissivity; Foam emissivity; Whitecap fraction

16. SECURITY CLASSIFICATION OF:			**17. LIMITATION OF ABSTRACT**	**18. NUMBER OF PAGES**	**19a. NAME OF RESPONSIBLE PERSON**
a. REPORT	**b. ABSTRACT**	**c. THIS PAGE**			Magdalena Anguelova
U	U	U	U	38	**19b. TELEPHONE NUMBER** *(include area code)* (202) 404-6342

Standard Form 298 (Rev. 8-98)
Prescribed by ANSI Std. Z39.18

This page intentionally left blank.

CONTENTS

This page intentionally left blank.

ANALYTICAL FORMULATIONS FOR FOAM EMISSIVITY MODELING AND THEIR NUMERICAL IMPLEMENTATIONS

1. INTRODUCTION

An international science team was formed in 2019 under the auspices of the International Space Science Institute (ISSI) to develop a radiative transfer model (RTM) of reference quality for the ocean surface emissivity e and backscatter from L band to infrared (IR) frequencies (1 GHz to 100 THz) [1]. The ISSI provided forum for the science team to discuss the status of current RTMs, plan project approach, report work progress, and present project results by funding six workshops in in-person, virtual, and hybrid formats (https://www.issibern.ch/teams/oceansurfemiss/). The result of this project is the Passive and Active Reference Microwave to Infrared Ocean (PARMIO) model with code provided as community software on GitHub (github.com).

Modeling the sea foam contribution to e is one of several elements in PARMIO. As part of the ISSI science team, our specific objective was developing efficient, accurate, and reliable code for the foam emissivity e_f. The approach to achieving this objective comprised four tasks: (a) Comparing and evaluating existing foam emissivity models; (b) Optimizing the foam emissivity model by tuning the foam properties parameters; (c) Assessing the performance of the tuned foam emissivity model using satellite observations; and (d) Incorporating the updated foam emissivity model in PARMIO.

This Memorandum Report documents the results of our effort on the first task (a). Tasks (b)–(d) have been reported in [2] and [3]. Extended journal publication on (b) and (c) is forthcoming.

Building on the incoherent approach to RT modeling [4], Anguelova and Gaizer [5] model foam emissivity e_f at WindSat nominal frequencies 6 to 37 GHz with a focus on the vertical stratification of the foam properties in sea foam layers [6]. Naval Research Laboratory (NRL) implemented this foam emissivity model in IDL (Interactive Data Language). Yin et al. [7] adjusted the model of [5] for L band (1.4 GHz) and incorporated it in the Laboratoire d'Océanographie et du Climat full (i.e., ocean and atmosphere) RTM called LOCEAN. Updated version of LOCEAN RTM, implemented in Fortran language (hereafter F90), was recently assessed by [8].

For task (a), we compared the current implementations of e_f, namely the IDL code of NRL and the F90 code of LOCEAN. Examination of the formulae used in the IDL and F90 codes showed that the NRL and LOCEAN implementations had four main differences:

(i) The choice of a seawater permittivity model;
(ii) The formulation of the incoherent approach for e_f ;
(iii) The calculation of the Fresnel reflectivity at the bottom of the foam layer;
(iv) The use of different numerical integration approximations.

For point (i) above, LOCEAN F90 code used the permittivity model [9] (hereafter referred to as KS77), while the NRL IDL code used [10] (hereafter S97). Both implementations extended these permittivity models beyond their frequency range of applicability. Permittivity model KS77 is applicable for 1 to 3 GHz, but LOCEAN F90 code applied it for frequencies up to 89 GHz [8]. Permittivity model S97 is applicable for 5 to 100 GHz, but NRL IDL code applied it down to 1 GHz [5].

For point (iv), the NRL code used the trapezoidal rule while LOCEAN code used the Simpson rule.

For the implementation of the full PARMIO, we needed to reconcile these four differences in order to decide which models, approaches, and formulae to use in the unified F90 code for the full PARMIO. We had ready decisions for points (i) and (iv). We adopted the double Debye model for the permittivity of seawater ε as parameterized by [11, 12] (hereafter MW). We used the Simpson rule for integration because it has smaller error than that of the trapezoidal rule.

For points (ii) and (iii), we needed first to verify the analytical expressions used for e_f and then to examine their numerical implementations in the NRL and LOCEAN codes. The following describes these two aspects, analytical (section 3) and then numerical (section 4). Sensitivity studies for varying conditions and parameters are also given (section 5). We start this exposé with a background information, which introduces the main terms and variables describing a stratified foam layer (section 2).

2. BACKGROUND: SEA FOAM PROPERTIES IN A STRATIFIED FOAM LAYER

The photograph here (Photo 1) shows a foam layer formed under a breaking wave. The stratification of bubbles by size, and the related differences in the bubble wall thicknesses, yield a profile in the foam void fraction (defined as the air content in the air-seawater mixture comprising the foam). We present the foam void fraction with an exponential profile:

$$f_a(z) = a_V - m \exp(b_V z) \tag{1a}$$

$$a_V = v_{af} + m \tag{1b}$$

$$b_V = \frac{1}{t}.\ln\left(\frac{a_V - v_{fw}}{m}\right) \tag{1c}$$

Here, m is a parameter that controls the shape of the profile and t is the foam layer thickness. Coefficients a_V and b_V are determined from the following boundary conditions:

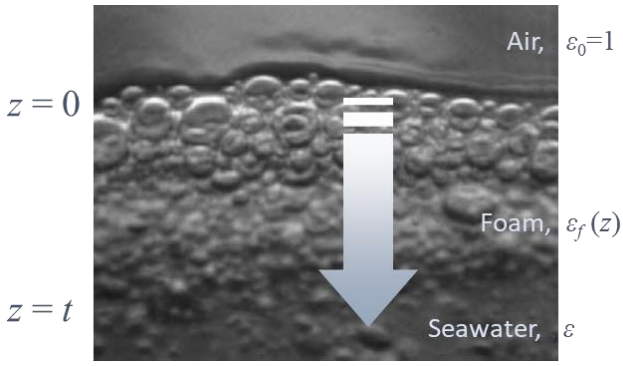

Photo 1 — Foam layer comprising bubbles stratified by size. The arrow shows the resulting vertical profile of foam void fraction and dielectric properties from the air-foam boundary down to foam-seawater boundary.

$$f_a(z) = \begin{cases} v_{af} & z = 0 \\ v_{fw} & z = t \end{cases} \tag{2}$$

where v_{af} and v_{fw} are the upper and lower limits of $f_a(z)$ at (respectively) the air—foam (top) and foam—water (bottom) boundaries of the foam layer.

The vertical void fraction profile $f_a(z)$ makes the foam layer dielectrically inhomogeneous with a vertically varying complex dielectric constant (permittivity) of foam $\varepsilon_f(z) = \varepsilon_f'(z) - j\,\varepsilon_f''(z)$, where $j = \sqrt{-1}$. We obtain the foam permittivity $\varepsilon_f(z)$ with the Refractive model, a quadratic mixing rule well suited for sea foam [13]:

$$\varepsilon_f(z) = \left[f_a(z)\varepsilon_0^{\frac{1}{2}} + \big(1 - f_a(z)\big)\varepsilon^{\frac{1}{2}} \right]^2 \tag{3}$$

where $\varepsilon_0 = 1$ is the air permittivity and ε is the seawater permittivity.

Sea foam is a lossy medium due to the presence of seawater in it. Having the foam permittivity $\varepsilon_f(z)$, we describe foam using the most general representations of attenuation and phase factors in a medium [4, p. 67], respectively:

$$\alpha(z) = k_0 \left| \mathrm{Im}\left\{ \sqrt{\varepsilon_f(z)} \right\} \right| \tag{4a}$$

$$\beta(z) = k_0 \mathrm{Re}\left\{ \sqrt{\varepsilon_f(z)} \right\} \tag{4b}$$

where $k_0 = 2\pi F/c$ is the radiation wave number in air for frequency F; c is speed of light in air [for $c = 299792458$ m/s in vacuum and air index of refraction of 1.000293, in air we use $c \cong 299704644.54$ m/s (= 299792458/1.000293)].

Due to the vertically varying losses, from air to foam to seawater or backwards, incident or emitted electromagnetic (EM) radiation refracts while propagating through a stratified foam layer. For an incidence angle in air θ (Photo 2), the refraction angle in foam changes in foam layer depth $\theta_f(z)$ following Snell law [4, Section 2-8]:

$$\theta_f(z) = \arctan\left\{ \frac{\sqrt{2}\, k_0 \sin(\theta)}{\left[(p^2+q^2)^{1/2} + q \right]^{1/2}} \right\} \tag{5}$$

with parameters p and q in the form:

$$p(z) = 2\alpha\beta \tag{6a}$$

$$q(z) = \beta^2 - \alpha^2 - k_0^2 \sin^2(\theta) \tag{6b}$$

With the material and dielectric properties of the foam layer defined, now we can describe the radiative transfer processes contributing to the foam emissivity.

3. RESULTS: ANALYTICAL EXPRESSIONS

We present first the analytical formulation for the incoherent foam emissivity e_f (section 3.1), followed by the formulae for the Fresnel coefficient at the foam layer boundaries (section 3.2). In these sections, we often refer to Appendices A and B, thus it would be instructive to first review the appendices. We finish with comparing the expressions in sections 3.1 and 3.2 to those published (section 3.3).

3.1 Incoherent approach for foam emissivity

The foam emissivity model that we use for the ISSI PARMIO builds on the incoherent approach [4, section 4-14.2]. Appendix A shows the formulation and derivation of the expressions for incoherent emissivity in notations following [4]. Here, we cast these expressions in notations specific to foam. To this end, Photo 2 gives the variables characterizing the air-foam-seawater system corresponding to the notations of the 3-layered system shown in Figure A.2. The use of both foam-specific notations and notations from [4] helps to avoid misunderstanding when parsing the implementation code (section 4). Beside notations, the other significant difference between the formulations in Appendix A and in this section is that [4] expressions are applicable for a homogeneous layer, while the expressions given here are for non-homogeneous, vertically stratified layer.

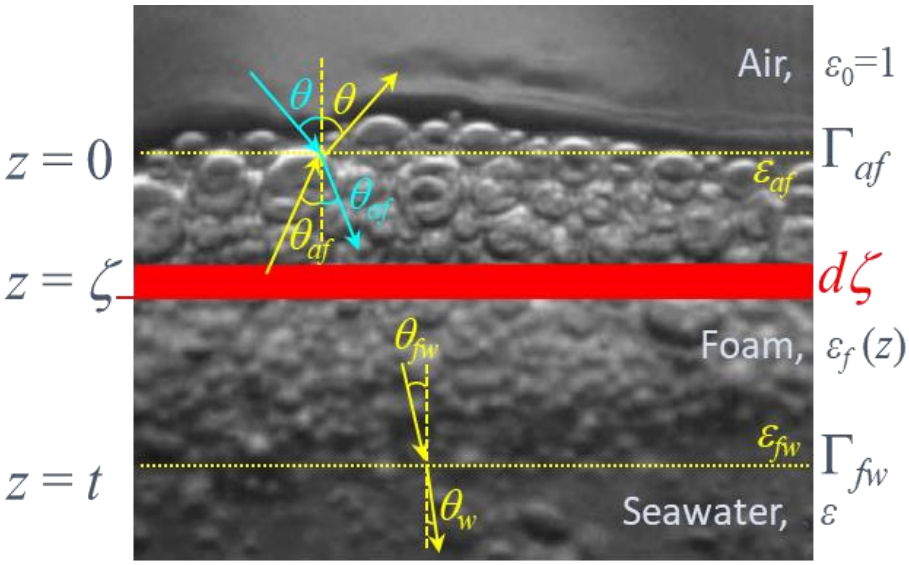

Photo 2 — Variables characterizing the air-foam-seawater system corresponding to the notations for a 3-layered system as shown in Figure A.2

The incoherent emissivity $e_i(\theta, p)$ of a homogeneous layer emitting in direction θ at horizontal or vertical polarizations $p = \mathrm{H}, \mathrm{V}$ has a closed form solution (A.33). As (A.8) shows, $e_i(\theta, p)$ contains upward and downward emissions from the layer (foam in our case) and upward emission from the underlying layer (seawater in our case). A foam-seawater system has the same contributions to the ocean surface emissivity as those shown with (A.8), namely:

$$T_{Bf}(\theta, p) = T_{B\,foam}(\theta, p) + T_{B\,water}(\theta, p) = T_{Uf}(\theta, p) + T_{Df}(\theta, p) + T_{Bw}(\theta, p) \qquad (7)$$

When the layer comprises sea foam with stratified properties (section 2), the closed form (A.33) is not directly applicable. Rather, we need to consider that the foam coefficients of extinction k_{ef}, absorption k_{af}, and scattering k_{sf} are vertically non-uniform. We account for this with a modification of (A.1) to include the profiles of these coefficients:

$$k_{ef}(z) = k_{af}(z) + k_{sf}(z) \tag{8}$$

The foam attenuation factor $\alpha_f(z)$ determines the absorption in the foam layer, thus, using (4a), the foam absorption coefficient is:

$$k_{af}(z) = 2\,\alpha_f(z) \tag{9}$$

The scattering in foam is negligible or at most 15% for frequencies from 1.4 to 37 GHz [13], therefore $k_{ef}(z) \cong k_{af}(z)$. For higher frequencies, foam scattering can be determined with the Mie theory [14] and thus provide formulation for $k_{sf}(z)$ in (8). The attenuation and phase factors in foam, $\alpha_f(z)$ and $\beta_f(z)$ respectively, can be used to determine the refractive angle in foam $\theta_f(z)$ with (5) and (6). With all these, we modify the closed-form optical depths (A.9) and (A.15) for a homogeneous layer to the upward and downward emissions in stratified foam layer as follows:

$$\tau_{Uf}(0,z) \equiv \tau_{s2}(0,z) = \int_0^z k_{ef}(\zeta)\sec\Big(\theta_f(\zeta)\Big)\,d\zeta = 2\int_0^z \alpha_f(\zeta)\sec\Big(\theta_f(\zeta)\Big)\,d\zeta \tag{10a}$$

$$\tau_{Df}(z,t) \equiv \tau_{s2}(z,t) = \int_z^t k_{ef}(\zeta)\sec\Big(\theta_f(\zeta)\Big)\,d\zeta = 2\int_z^t \alpha_f(\zeta)\sec\Big(\theta_f(\zeta)\Big)\,d\zeta \tag{10b}$$

The upward and downward emissions (A.10) and (A.16) then change for foam layer with thermodynamic temperature T as follows:

$$T_{sU}\big(\theta_f,0\big) \equiv T_{s2}(\theta_2,0) = T\int_0^t k_{af}(\zeta)\sec\Big(\theta_f(\zeta)\Big)\,e^{-\tau_{Uf}(0,\zeta)}d\zeta \tag{11a}$$

$$T_{sD}\big(\theta_f,t\big) \equiv T_{s2}(\theta_2,t) = T\int_0^t k_{af}(\zeta)\sec\Big(\theta_f(\zeta)\Big)\,e^{-e^{-\tau_{Df}(\zeta,t)}}d\zeta \tag{11b}$$

Because in non-uniform foam layer the emitting strata above and below each position z (section A.1) have different dielectric properties, it is not immediately clear from (10) whether $\tau_{Uf}(0,z) = \tau_{Df}(z,t)$. This is also the reason that in the integrands of (11) there are specific values $\tau_{Uf}(0,\zeta)$ and $\tau_{Df}(\zeta,t)$ for each integration position ζ covering the range $(0,t)$. The foam layer contributions $T_{sU}\big(\theta_f,0\big)$ and $T_{sD}\big(\theta_f,t\big)$ are counterparts of T_{s2} in (A.25) and (A.27). However, in a non-uniform foam layer, we cannot obtain their closed form solutions as this is done with (A.14) and (A.18) for a homogeneous layer. Instead, we need to integrate (11) numerically. In this sense, expressions (7) to (11) represent a more general formulation of the incoherent approach compared to the special case for homogeneous layer given in Appendix A.

The seawater upward emission is still presented with (A.21). Assuming the layered system isothermal, with seawater and foam both having thermodynamic temperature T, we write:

$$T_{sw}(\theta_w,t) \equiv T_{s3}(\theta_3,t) = T \tag{11.c}$$

3.2 Fresnel reflectivity at foam-water boundary

The incoherent approach to obtaining emissivity of a layered system (section A.2) also incorporates the multiple reflections and transmissions of the emission contributions at the layer boundaries (section A.2.3). The Fresnel reflectivity is thus a part of the final formulation of the incoherent emissivity.

Having $T_{sU}(\theta_f, 0)$, $T_{sD}(\theta_f, t)$, and $T_{sw}(\theta_w, t)$ as analogs to T_{s2} in (A.25) and (A.27) and T_{s3} in (A.28), respectively, we next need to determine the "multi" factors attached to T_{s2} and T_{s3} in order to obtain the terms in (7) from (11):

$$T_{Uf}(\theta, p) = \frac{1-\Gamma_1}{1-\Gamma_1\Gamma_2/L_2^2}\ T_{sU}(\theta_f, 0) \quad = m_U T_{sU}(\theta_f, 0) \tag{12.a}$$

$$T_{Df}(\theta, p) = \frac{\Gamma_2(1-\Gamma_1)}{\mathrm{L}_2(1-\Gamma_1\Gamma_2/L_2^2)}\ T_{sD}(\theta_f, t) = m_D T_{sD}(\theta_f, t) \tag{12b}$$

$$T_{Bw}(\theta, p) = \frac{(1-\Gamma_1)(1-\Gamma_2)}{\mathrm{L}_2(1-\Gamma_1\Gamma_2/L_2^2)} T_{sw}(\theta_w, t) = m_w T_{sw}(\theta_w, t) \tag{12c}$$

To obtain the "multi" factors m_U, m_D, and m_w in (12), we need Γ_1, Γ_2, and L_2 in terms of foam layer variables. In (12), the loss factor L_2 is determined from the exponential losses over the entire foam layer, i.e., following (A.12) and (A.13), we have:

$$L_f(0, t) \triangleq \frac{1}{\tau_f(0,t)} = e^{\tau_{f\theta}(0,t)} \tag{13}$$

where $\tau_{f\theta}(0, t)$ is the optical depth of the entire stratified foam layer along refractive path determined by θ_f. Similar to (10), but for all positions in the range $(0, t)$, we have:

$$\tau_{f\theta}(0, t) = 2\int_0^t \alpha_f(\zeta) \sec\left(\theta_f(\zeta)\right) d\zeta \tag{14}$$

To determine the foam-specific forms of Γ_1 and Γ_2 in (12), we cast the expressions derived in Appendix B in terms of the air-foam-seawater system variables (section 2). For Γ_1— denoted Γ_{af} at the air-foam boundary (Photo 2)—we use (B.12) to present medium 1 to medium 2 propagation with the following substitutions: $\varepsilon_2 = \varepsilon_f\big|_{z=0} \equiv \varepsilon_{af}$ and $\theta_1 \equiv \theta$:

$$r_{af}(\theta, \mathrm{V}) = \left|\frac{\varepsilon_{af}\cos\theta - \sqrt{\varepsilon_{af} - \sin^2\theta}}{\varepsilon_{af}\cos\theta + \sqrt{\varepsilon_{af} - \sin^2\theta}}\right| \tag{15a}$$

$$r_{af}(\theta,\mathrm{H}) = \left| \frac{\cos\theta - \sqrt{\varepsilon_{af} - \sin^2\theta}}{\cos\theta + \sqrt{\varepsilon_{af} - \sin^2\theta}} \right| \tag{15b}$$

Note that the propagation direction (from medium 1 to medium 2 or vice versa) does not change the result for Γ_{af} by virtue of (B.7).

For Γ_2—denoted Γ_{fw} at the foam-seawater boundary (Photo 2)—we use (B.13) to present propagation from medium 2 to medium 3 with the following substitutions: $\varepsilon_2 = \varepsilon_f\big|_{z=t} \equiv \varepsilon_{fw}$ and $\theta_2 = \theta_f\big|_{z=t} \equiv \theta_{fw}$:

$$r_{fw}(\theta_{fw},\mathrm{V}) = \left| \frac{\varepsilon\cos\theta_{fw} - \sqrt{\varepsilon_{fw}}\sqrt{\varepsilon - \varepsilon_{fw}\sin^2\theta_{fw}}}{\varepsilon\cos\theta_{fw} + \sqrt{\varepsilon_{fw}}\sqrt{\varepsilon - \varepsilon_{fw}\sin^2\theta_{fw}}} \right| \tag{16a}$$

$$r_{fw}(\theta_{fw},\mathrm{H}) = \left| \frac{\sqrt{\varepsilon_{fw}}\cos\theta_{fw} - \sqrt{\varepsilon - \varepsilon_{fw}\sin^2\theta_{fw}}}{\sqrt{\varepsilon_{fw}}\cos\theta_{fw} + \sqrt{\varepsilon - \varepsilon_{fw}\sin^2\theta_{fw}}} \right| \tag{16b}$$

We can present Γ_{fw} in terms of θ instead of θ_{fw} using (B.14). Though (B.14) was derived for a homogeneous layer, it is applicable for varying $\theta_f(z)$ due to (B.5), which can be generalized for l sublayers each with specific ε_l and θ_l:

$$\sin\theta_l = \sqrt{\frac{\varepsilon_{l-1}}{\varepsilon_l}}\sin\theta_{l-1} \tag{17a}$$

$$\cos\theta_l = \frac{1}{\sqrt{\varepsilon_l}}\sqrt{\varepsilon_l - \varepsilon_{l-1}\sin^2\theta_{l-1}} \tag{17b}$$

Consecutive use of (17) in the general formula (B.2) starting at $\theta_f\big|_{z=t}$ and going upward to $\theta_f\big|_{z=0}$ gives:

$$Z_l = \frac{1}{\varepsilon_l}\sqrt{\varepsilon_l - \varepsilon_1\sin^2\theta_1} \tag{18}$$

where ε_1 and θ_1 are the permittivity and incidence angle in the air above the layer. Therefore, from (B.14), using $\varepsilon_l = \varepsilon_f\big|_{z=t} \equiv \varepsilon_{fw}$, $\varepsilon_1 = 1$, and $\theta_1 \equiv \theta$ (Photo 2), we have:

$$r_{fw}(\theta,\mathrm{V}) = \left| \frac{\varepsilon_{fw}\sqrt{\varepsilon - \sin^2\theta} - \varepsilon\sqrt{\varepsilon_{fw} - \sin^2\theta}}{\varepsilon_{fw}\sqrt{\varepsilon - \sin^2\theta} + \varepsilon\sqrt{\varepsilon_{fw} - \sin^2\theta}} \right| \tag{19a}$$

$$r_{fw}(\theta, \mathrm{H}) = \left| \frac{\sqrt{\varepsilon_{fw} - \sin^2\theta} - \sqrt{\varepsilon - \sin^2\theta}}{\sqrt{\varepsilon_{fw} - \sin^2\theta} + \sqrt{\varepsilon - \sin^2\theta}} \right| \tag{19b}$$

With the foam boundary reflectivity Γ_{af} and Γ_{fw} determined, the forms of factors m_U, m_D, and m_w in (12) are defined as follows:

$$m_U = \frac{1-\Gamma_{af}}{1-\Gamma_{af}\Gamma_{fw}/L_f^2} \tag{20a}$$

$$m_D = \frac{\Gamma_{fw}}{\mathrm{L}_f} \frac{1-\Gamma_{af}}{1-\Gamma_{af}\Gamma_{fw}/L_f^2} = \frac{\Gamma_{fw}}{\mathrm{L}_f} m_U \tag{20b}$$

$$m_w = \frac{1-\Gamma_{fw}}{\mathrm{L}_f} \frac{1-\Gamma_{af}}{1-\Gamma_{af}\Gamma_{fw}/L_f^2} = \frac{1-\Gamma_{fw}}{\mathrm{L}_f} m_U \tag{20c}$$

3.3 Published formulations

The incoherent approach (Appendix A) has been applied to obtain the foam emissivity e_f for a foam layer with a void fraction profile. Here we summarize the documentation of e_f models in the peer-reviewed literature.

3.3.1 Anguelova and Gaiser (2013)

Anguelova and Gaiser [5, their Eqs. 1-6], combined with A.1-A.6, obtain e_f using the general formulation of the incoherent approach (7) to (11) for a stratified foam layer [defined with (1) to (6) in section 2].

Model [5, Eq. (A.7)] present the boundary reflectivity Γ_{af} and Γ_{fw} in terms of θ. Note that their expression (A.7b) in [5] for Γ_{fw} uses the correct form (19) with the correct incidence angle θ, however this expression has an error: the presence of product $\varepsilon\,\varepsilon_{fw}$ in the radicals is not correct.

The error in Γ_{fw} was traced to the use of (4.132) in [4] with substitution of variables; this approach is demonstrated in section B.2 for expression (B.8). However, in section B.2, we did this substitution when using the most general expressions (B.6), while (4.132) is for the case of air-medium boundary with $\varepsilon_1 = 1$ incorporated [the special case given with (B.12)]. The result of substituting variables in the special case formula instead of in the general formula is that ε_f is not removed when the foam refractive angle is expressed in terms of the incidence angle in air with the Snell law, i.e., $\theta_f(\theta)$; thus, a product $\varepsilon\,\varepsilon_{fw}$ comes about.

3.3.2 Yin et al. (2016)

Yin et al. [7, their Eq. B.6] obtain e_f using the simplified closed-form formulation (hereafter referred to as semi-closed form) of the incoherent approach (A.34b). Model [7] does not use integrations (10) and (11).

Model [7, their Eq B.7] use the stratified foam properties to obtain the optical depth of the full foam layer τ_f. This τ_f contributes to the foam emissivity via the exponential losses τ in [7, their eq. (B.6)]. Note that (B.6) in [7] has a typo in the denominator; it has to be $(1 - \Gamma_1\Gamma_2\tau^2)$, not $(1 - \Gamma_1\Gamma_2/\tau^2)$.

Model [7] give the foam boundary reflectivity Γ_{af} and Γ_{fw} with their Eqs. (B.13) to (B.17). Foam permittivity ε_f is used in these expressions, but it is not clear which value of ε_f is used, while (15) and (19) show that different values of ε_f must be used for the reflectivity at each boundary.

The foam-seawater reflectivity Γ_{fw} (Eqs. B.15 and B.16 in [7]) is given in terms of the foam refracted incident angle θ_f. However, the expression is not in the correct form (16); instead (19) is used, which is the form derived for Γ_{fw} in terms of the incidence angle in the air θ. In other words, Eqs. (B.15) and (B.16) in [7] must use θ, as in their Eqs. (B.13) and (B.14).

While the formulae of the published foam emissivity models may have some typos and errors, it is more important to see if those inaccuracies have found their way in the implementation codes. We present this in the next section.

4. RESULTS: IMPLEMENTATIONS

Here we parse the codes implementing the expressions used for the incoherent foam emissivity (section 3.1) and for the foam reflectivity at both the top (air-foam) and bottom (foam-seawater) boundaries (section 3.2).

4.1 NRL IDL code

The NRL implementation of the foam emissivity has coded the generalized formulation for incoherent emissivity given with formulae (7)–(14) and (20) applied for stratified foam layer described with (1) to (6). The foam-seawater reflectivity Γ_{fw} is coded with the error described in section (3.3.1).

4.2 LOCEAN F90 code

The LOCEAN implementation of the foam emissivity (F90 code is given in Appendix C) mostly follows the formulation given in [7]. However, a modified closed form (A.33) (not A.34b) is used, i.e., semi-closed form. This is useful for future addition of scattering in the calculations via the single scattering albedo a_2. Currently a_2 is set to 0.

The use of (A.33) means that the integrations (10) and (11) are not used in the LOCEAN foam emissivity. The only integration over stratified foam properties is done for τ_f, which is then used for the exponential losses τ (i.e., the loss factor L_f).

The foam boundary reflectivity is calculated with subroutine 'ReflTransm_PlanarBoundary' (Appendix C). Coded in the subroutine are the general expressions (B.5) and (B.6) with ε_1, ε_2, and θ_1 (the incidence angle in air) as input parameters for the subroutine. Subroutine 'IncohEmissivity_TwoLayer' prepares the input variables for two calls to subroutine 'ReflTransm_PlanarBoundary', once for the air-foam boundary to get Γ_{af}, then a second call for the foam-seawater boundary to get Γ_{fw}.

The input parameters for the first call to 'ReflTransm_PlanarBoundary' (documented in the code as '12 Interface') are $\varepsilon_1 = 1$ (variable eps1 in F90 code), $\varepsilon_2 = \varepsilon_{af}$ (eps2 = sigfoam1 in F90), and $\theta_1 = \theta$ (theta_i in F90). With these input parameters, the coded general formulae (B.6) become exactly as (15). Thus, the coded expressions with these input variables calculate Γ_{af} correctly.

The input parameters for the second call to 'ReflTransm_PlanarBoundary' (documented in the code as '23 Interface'), as traced from 'IncohEmissivity_TwoLayer', are $\varepsilon_1 =$ eps2 = sigfoam1 $= \varepsilon_{af}$, $\varepsilon_2 =$ eps3 = sigfoam2 $= \varepsilon_{fw}$. There are two operations for the incident angle performed in this subroutine call. First, 'IncohEmissivity_TwoLayer' uses the incidence angle in air $\theta_1 = \theta$ = theta_i to get from the Snell law refractive angle theta2 $=$ asin$\left(\sqrt{\frac{\varepsilon_{af}}{\varepsilon_{fw}}}\sin\,\theta\right)$; let's denote this first refraction θ_{f1}. Variable theta2 is input to 'ReflTransm_PlanarBoundary' where it is used in Snell law once again to obtain sin_theta2 $= \sqrt{\frac{\varepsilon_{af}}{\varepsilon_{fw}}}\sin(\theta_{f1})$; let's denote this second refraction $\sin(\theta_{f2})$. We then have cos_theta2 $= \cos(\theta_{f2}) = \frac{1}{\sqrt{\varepsilon_{fw}}}\sqrt{\varepsilon_{fw} - \varepsilon_{af}\sin(\theta_{f1})}$; (17) corroborates these expressions. With these input parameters, the coded general formulae (B.6) give the following:

$$\text{rhoV} \equiv r_{fw}(\theta_f, \text{H}) = \left|\frac{\varepsilon_{fw}\cos\theta_{f1} - \sqrt{\varepsilon_{af}}\sqrt{\varepsilon_{fw} - \varepsilon_{af}\sin^2\theta_{f1}}}{\varepsilon_{fw}\cos\theta_{f1} + \sqrt{\varepsilon_{af}}\sqrt{\varepsilon_{fw} - \varepsilon_{af}\sin^2\theta_{f1}}}\right| \tag{21a}$$

$$\text{rhoH} \equiv r_{fw}(\theta_f, \text{H}) = \left|\frac{\sqrt{\varepsilon_{af}}\cos\theta_{f1} - \sqrt{\varepsilon_{fw} - \varepsilon_{af}\sin^2\theta_{f1}}}{\sqrt{\varepsilon_{af}}\cos\theta_{f1} + \sqrt{\varepsilon_{fw} - \varepsilon_{af}\sin^2\theta_{f1}}}\right| \tag{21b}$$

Expressions (21) have the form of (16), which is in terms of the foam-seawater incidence angle θ_{fw}, but (21) uses the first refractive angle θ_{f1} (for the air-foam boundary) instead of the second refractive angle θ_{f2} (for the foam-seawater boundary). Note that air-foam refractive angle would be $\sin(\theta_{af}) = \sqrt{\frac{1}{\varepsilon_{af}}}\sin(\theta)$, and thus $\theta_{f1}(\theta)$ is different from $\theta_{af}(\theta)$. Similarly, foam-seawater refractive angle would be $\sin(\theta_w) = \sqrt{\frac{\varepsilon_{wf}}{\varepsilon}}\sin(\theta_{fw})$, and thus $\theta_{f2}(\theta_{fw})$ is different from $\theta_w(\theta_{fw})$. In addition to the imprecise angles, the subroutine input parameters also render imprecise permittivities in (21); instead of permittivity of air ($= 1$) and seawater ($= \varepsilon$), we have their approximate values as $\varepsilon_{af} \approx 1$ and $\varepsilon_{fw} \approx \varepsilon$.

To provide (16) with the correct values, the input parameters in the second call to 'ReflTransm_PlanarBoundary' should be as follows:

- for input eps1 [(ε_1 in (B.6)], we need ε_{fw} = sigfoam2= eps3;
- for input eps2 [(ε_2 in (B.6)], we need ε = epsi;
- for input theta1d [(θ_1 in (B.6)], we need $\theta_{fw} \equiv \theta_f\big|_{z=t} = \theta_f(\varepsilon_{fw})$.

With these input parameters, the coded general formulae (B.6) become exactly as (16). Appendix C describes the changes in the F90 code to provide the correct input variables.

5. RESULTS: SENSITIVITY STUDIES

Here, we analyze three aspects of the LOCEAN F90 and NRL IDL implementations. First, we reconcile the implementation differences of the F90 and IDL codes (section 5.1). Next, we compare the outputs of

the semi-closed form (F90) and the generalized formulation (IDL) for different environmental conditions (section 5.2). Finally, we investigate the sensitivity of the LOCEAN and NRL models to variations of foam properties (section 5.3).

We run all code versions at a fixed incidence angle θ = 55° for the six frequencies used in LOCEAN [8]: 1.4, 6.9, 10.6, 18.7, 36.5, 89 GHz. The foam layer properties are listed in Table 1.

Table 1 — Fixed parameters for foam fraction profile (sections 5.1 and 5.2). The values in parentheses are used for the sensitivity study (section 5.3).

Foam void fraction $f_a(z)$		
Variable (symbol)	Value	Units
Layer thickness (t)	2 (1, 4)	cm
Upper profile limit (v_{af})	0.95 (0.85, 0.75)	
Lower profile limit (v_{fw})	0.01	
Profile shape (m)	1	

In all cases, we assess how much each code modification affects the resulting foam emissivity e_f. We do that by quantifying the discrepancy between new and previous results in terms of percent difference (PD). We determine the PD (in %) between two values x_1 and x_2 as the ratio of their difference and their average:

$$\text{PD} = |x_1 - x_2|/[(x_1 + x_2)/2] * 100 \tag{22}$$

All figures show the frequency dependence of the variables (e_f or PD) because we are interested in the application of the foam emissivity models for a wide spectral range.

5.1 Reconciling F90 and IDL code implementations

We reconcile the differences between LOCEAN F90 and NRL IDL implementations one by one in order to assess how much each change affects the results. All calculations are at fixed sea surface temperature (SST) of 293 K (19.75 °C) and sea surface salinity (SSS) of 34 psu, same as those that [8] have used. Table 2 gives the main elements in each code (F90 and IDL) that we seek to reconcile, namely semi-closed form and generalized formulation for foam emissivity e_f calculations, integration rule, correct coding of Γ_2 , and seawater permittivity model (column headings 3 to 6 in the table). Each step in Table 2 shows (in red) which element was changed for each code version. The last column in Table 2 gives the average (for all frequencies) PD between F90 and IDL results for each modifying step; each new step is compared to the previous step.

As Table 2 shows, we start with the original implementations (Step 1, referred to as 'Orig'), for which all identified differences (Section 1) remain unchanged; i.e., we run the initial, original codes as they are. Figure 1 shows the frequency dependence of e_f from LOCEAN F90 (blue line) and NRL IDL (magenta line) for Step 1. With all differences in place, the discrepancy between the F90 and IDL implementations is less for V polarization (Figure 1a) than for H polarization (Figure 1b). Figure 2 shows these discrepancies in terms of PD (green line). The PD is maximum of 0.15% for V pol at 1.4 GHz and much lower for all other frequencies, while it is maximum of 1.45% for H polarization at 36.5 GHz; see Table 2 for the average PDs.

Table 2 — Elements comprising the code implementations (LOCEAN F90 and NRL IDL) and their modifications in steps.

Step #	Code	Foam emiss e_f	Integration	Coding Γ_2	Permittivity	PD (%)[1]
1 Orig	F90	Semi-closed form	Simpson	Input err	KS77	0.067 (V)
	IDL	General form	Trapezoid	Formula err	S97	0.921 (H)
2 Perm	F90	Semi-closed form	Simpson	Input err	MW	0.074 (V)
	IDL	General form	Trapezoid	Formula err	MW	1.019 (H)
3 Fix Γ_2	F90	Semi-closed form	Simpson	Input Fix	MW	0.061(V)
	IDL	General form	Trapezoid	Formula Fix	MW	1.011(H)
4 Int rule	F90	Semi-closed form	Simpson	Input Fix	MW	0.040 (V)
	IDL	General form	Simpson	Formula Fix	MW	0.307 (H)
5 e_f form	F90	Semi-closed form	Simpson	Input Fix	MW	0.024 (V)
	IDL	Semi-closed form	Simpson	Formula Fix	MW	0.291 (H)

[1]The color for each step matches the color of the respective line in Figure 2.

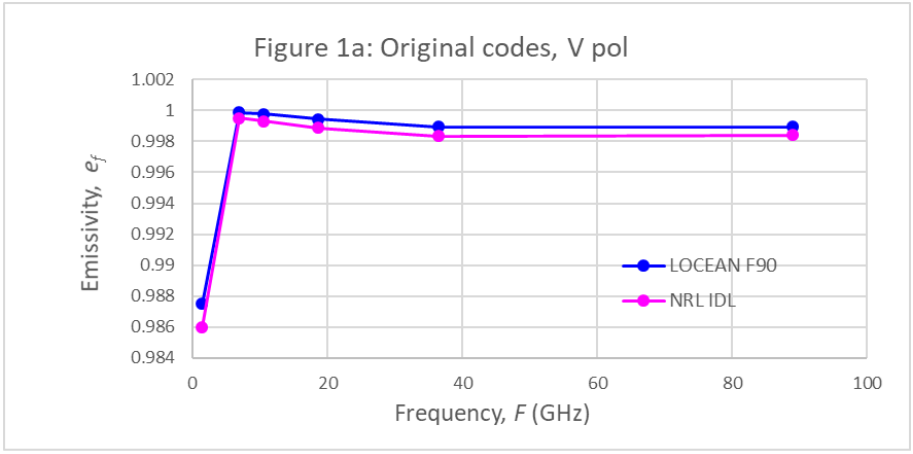

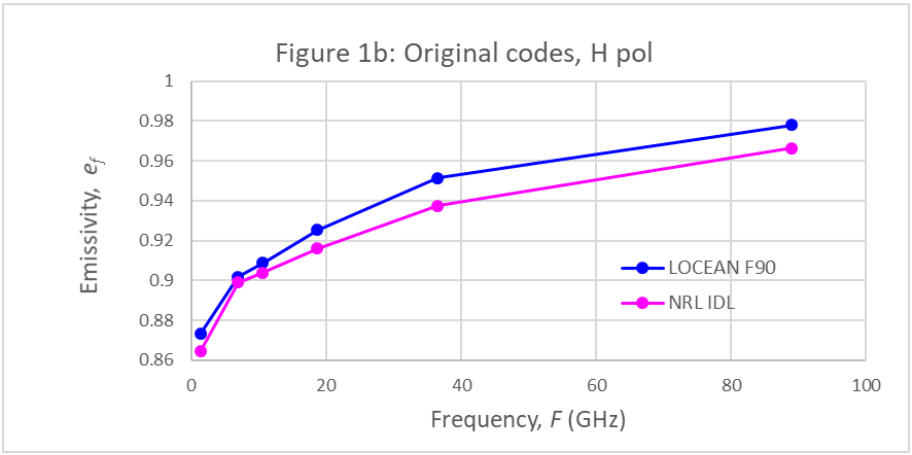

Fig. 1 — Frequency dependence of foam emissivity e_f from the original codes NRL IDL (magenta) and LOCEAN F90 (blue): (a) V pol; (b) H pol.

Step 2 in Table 2 (referred to as 'Perm') changes the permittivity model for the seawater. Permittivity model MW replaces model KS77 in the F90 code and model S97 in the IDL code. The use of a new permittivity model yields small yet noticeable changes (especially for L band) in the e_f values. Figure 2 shows PDs between the F90 and IDL codes: compare the magenta line (partially covered by the yellow line) to the green line. The changes between 'Orig' and 'Perm' steps is larger for H pol than for V pol (Figure 2). These results imply that, even beyond their range of applicability, the performance of the permittivity models KS77 and S97 is comparable to that of model MW for all frequencies.

Step 3 in Table 2 (referred to as 'Fix Γ_2') modifies different things in each code regarding the reflectivity Γ_2 at the foam-seawater boundary. It fixes the error in the formula in the IDL code (section 4.1) and the input variables for the subroutine in the F90 code (section 4.2). Analysis of the IDL results with and without the error in the Γ_2 formula shows that fixing the formula changes the IDL e_f values the most for the low frequencies, especially 1.4 GHz. The PD between the IDL codes with and without the error (not shown here) reaches 0.65% for V pol and 0.53% for H pol. We conjecture that the reason for the larger differences at low frequencies (but smaller differences at higher frequencies) is the effect of foam layer thickness on the foam emissivity values [15]. Namely, e_f is from the uppermost part of the foam layers at high frequencies; even for thin layers, this means mostly dry foam with high f_a values. At low frequencies, thin foam layers are more strongly affected by the seawater emissivity below the foam. Thus, inaccurate estimate of Γ_2 could affect e_f values when foam is not the sole contributor to the emissivity.

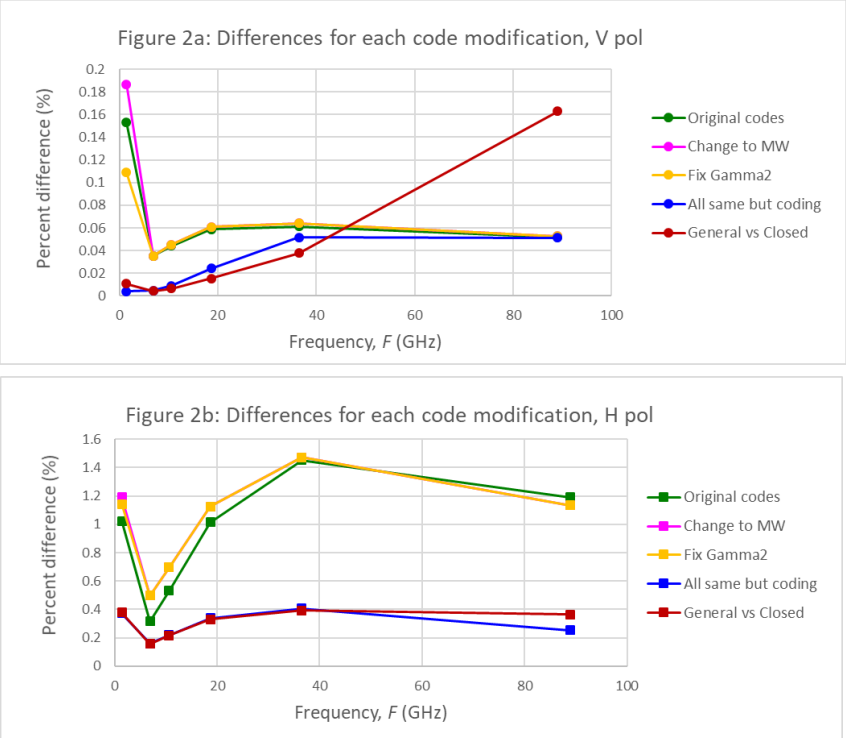

Fig. 2 — Frequency dependence of the percent difference for different changes in the code (Table 2). (a) V pol.; (b) H pol).

Analysis of the F90 results with incorrect and correct input variables (Appendix C) shows that modifying the input variables changes the F90 e_f values the most for the low frequencies, especially 1.4 GHz. The PD between the F90 codes with incorrect and correct input variables reaches 0.63% for V pol and 0.58% for H pol.

The PD between F90 and IDL codes after step 3 (Table 2) is shown in Figure 2 (yellow lines). The figure corroborates the conclusions of the individual (IDL or F90) analyses, namely that fixing the calculation of Γ_2 affects 1.4 GHz results the most, more so for H pol than for V pol (compare green and yellow lines in Figure 2). For higher frequencies, step 'Fix Γ_2' yields negligible changes compared to the previous results (from step 2); we see this from the overlap of the yellow and magenta lines in Figure 2.

Step 4 in Table 2 (referred to as 'Int rule') changes the trapezoidal integration scheme, used in the IDL code, to integration using the Simpson rule, thus matching the integration carried out in the F90 code. Table 2 shows that with this modification the only difference remaining between the F90 and the IDL codes is the formulation of the incoherent approach (semi-closed versus generalized forms, section 4). Figure 3 shows the frequency dependence of e_f and IDL implementations for V polarization is below 0.04% (Figure 2a, compare green and red lines) with exception for 89 GHz. The improvement is much better for H polarization (Figure 2b), which shows PD < 0.4%. Comparing the average PDs in Table 2 (last column) for each modification (steps 1 to 4) suggest that the largest improvement comes with the consistent use of the integration rule. Importantly, the small discrepancies at this stage of the F90 vs IDL comparison point that using the semi-closed form of the incoherent approach in the F90 code—as compared to the generalized formulation in the IDL code—is in fact quite a good approximation for the inhomogeneous foam layer emissivity e_f.

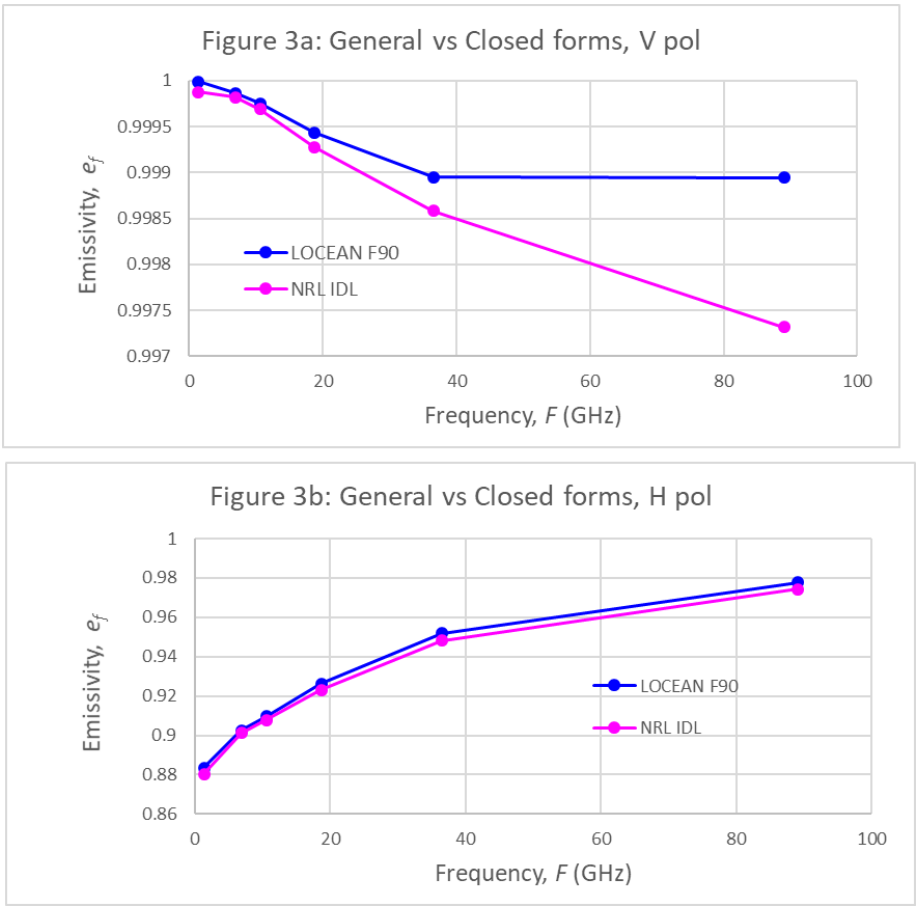

Fig. 3 — Frequency dependence of foam emissivity e_f general formulation in NRL IDL code (magenta) and closed form in LOCEAN F90 (blue): (a) V pol; (b) H pol.

Step 5 in Table 2 (referred to as 'e_f form') introduces the semi-closed form for e_f in the IDL code thus making all elements of both implementations the same. The result of this change brings the two implementations the closest to each other. Figure 2 (blue lines) shows that the PDs between the F90 and IDL codes are below 0.06% for V pol and below 0.4% for H pol for all frequencies. Because all elements are the same, these differences can be attributed to the coding itself using different programming languages (F90 versus IDL).

Figure 3 shows the frequency dependence $e_f(F)$ of the foam emissivity obtained with the reconciled (consistent) F90 and IDL implementations of the incoherent approach. The e_f values at V pol are higher than those at H pol. Noting the scales on the *y*-axes in Figure 3, it is clear that the foam emissivity is highly depolarized (compared to specular and rough surfaces) due to the random scattering in the foam. This suggests that the incoherent approach captures the radiative processes in foam well. The $e_f(F)$ trends for V and H pols are opposite: e_f values increase with F for H pol and decreases for V pol. In the following sensitivity investigations, we assess how the e_f values and the $e_f(F)$ trends change when parameters in the LOCEAN and NRL models vary.

5.2 Different environmental conditions

All results so far (section 5.1) are for typical oceanographic conditions with SSS = 34 psu and SST = 20 °C (19.75 °C to be exact, see section 5.1). Here, we look at the same foam and sensor parameters (Table 1), but change the SST and SSS values. Variations of the resulting e_f values are expected due to (3) and variations of the seawater permittivity ε with SST and SSS [16]. We use the F90 and IDL code versions of step 4 (Table 2) when all elements are the same but the formulations of the incoherent approach. The idea is to see how much the use of the semi-closed form of the incoherent approach (LOCEAN model in F90), instead of the generalized form (NRL model in IDL), would affect the e_f values for a range of environmental conditions. Differences arise because the two formulations use integration(s) over the foam layer differently (section 3.1). Again, we present the differences between the two models using PD as defined with (22).

Figure 4 shows the PDs between the semi-closed and general forms for e_f at V pol (Figure 4a) and H pol (Figure 4b) at fixed SSS = 34 psu and three different SST values (0, 20, and 30 °C). As before (section 5.1), the differences are less for V pol (PD < 0.25%) than for H pol (PD < 0.5%). The PD trends are non-monotonic. For both polarizations, there is a maximum change (a peak) for frequencies of 10 to 20 GHz at low SST = 0 °C (blue lines). For higher SST values, the maximum changes are for low frequencies (L, C and K bands) at H pol. While the overall changes are small (way below half of percent), the largest discrepancies between the semi-closed and general model formulations are at high frequencies (W band).

Figure 5 shows the PDs between the semi-closed and general forms for e_f at V pol (Figure 5a) and H pol (Figure 5b) at fixed SST = 20 °C and three different SSS values (30, 34, and 38 psu), which cover the range of salinity variations in the open ocean. As for the SST dependence (Figure 4), the differences are less for V pol (PD < 0.25%) than for H pol (PD < 0.5%). The discrepancies between the semi-closed and general model formulations are negligibly small for most frequencies at both V and H pols (all curves often overlap). The largest differences are for L band at H pol and W band for V pol.

With variations due to environmental parameters thus quantified, we can now investigate how changes in some of the parameters characterizing the foam layer affect the foam emissivity.

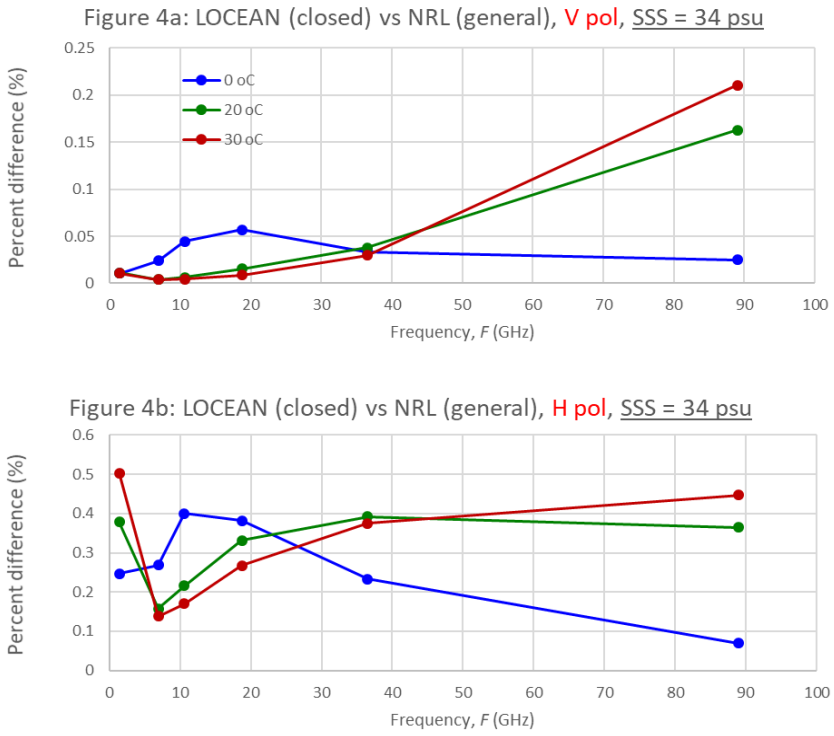

Fig. 4 — Frequency dependence of the percent difference between NRL IDL and LOCEAN F90 codes for fixed sea surface salinity of 34 psu at different sea surface temperatures (color legend): (a) V pol; (b) H pol.

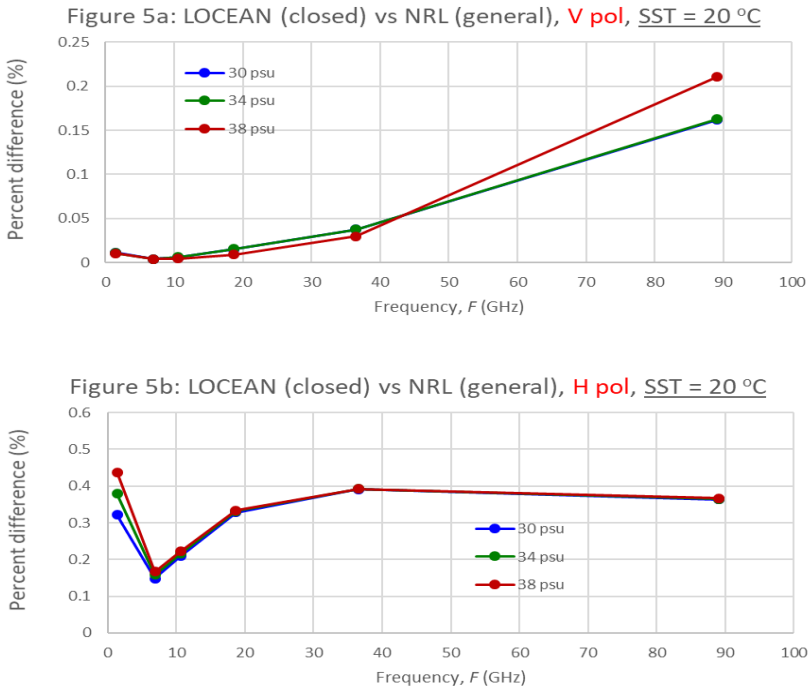

Fig. 5 — Frequency dependence of the percent difference between NRL IDL and LOCEAN F90 codes for fixed sea surface temperature of 20 °C at different sea surface salinity (color legend): (a) V pol; (b) H pol

5.3 Different foam properties

All sensitivity studies so far (sections 5.1 and 5.2) are for fixed foam layer properties, such as the void fraction profile and the foam layer thickness (Table 1). Here we look at fixed sensor and environmental parameters—namely, incidence angle θ = 55°, SST = 20 °C, and SSS = 34 psu—but change first the upper limit v_{af} of the void fraction profile (at fixed t, Table 1), then change t at fixed v_{af}.

As before, we use the F90 and IDL code versions at step 4 (Table 2) when all elements are the same but the formulations of the incoherent approach. We aim to assess how much the use of the semi-closed form of the incoherent approach (LOCEAN model in F90), instead of the generalized form (NRL model in IDL), would affect the e_f values for a range of foam layer properties. As before, we present the differences between the two models using PD from (22).

Figure 6 shows the frequency dependence of the foam emissivity at t = 2 cm and varying v_{af} values. Figures 6a and 6b are for LOCEAN and NRL models, respectively, at V pol; Figures 6c and 6d are for H pol. The chosen v_{af} values are the default upper limit (95%) of the f_a profile in the LOCEAN model [7]; the f_a value considered to separate wet and dry foam (85% according to [17]); and v_{af} representing a high bound of f_a in breaking waves (75% [13]). According to the figure, the foam emissivity decreases for lower v_{af}. The reason for this is the decrease of the impedance matching between the air and seawater as the foam becomes wetter and the dielectric contrast at the air-sea interface increases [6]. The result of this is an increase of the ocean surface reflectivity with commensurate decrease of the surface emissivity.

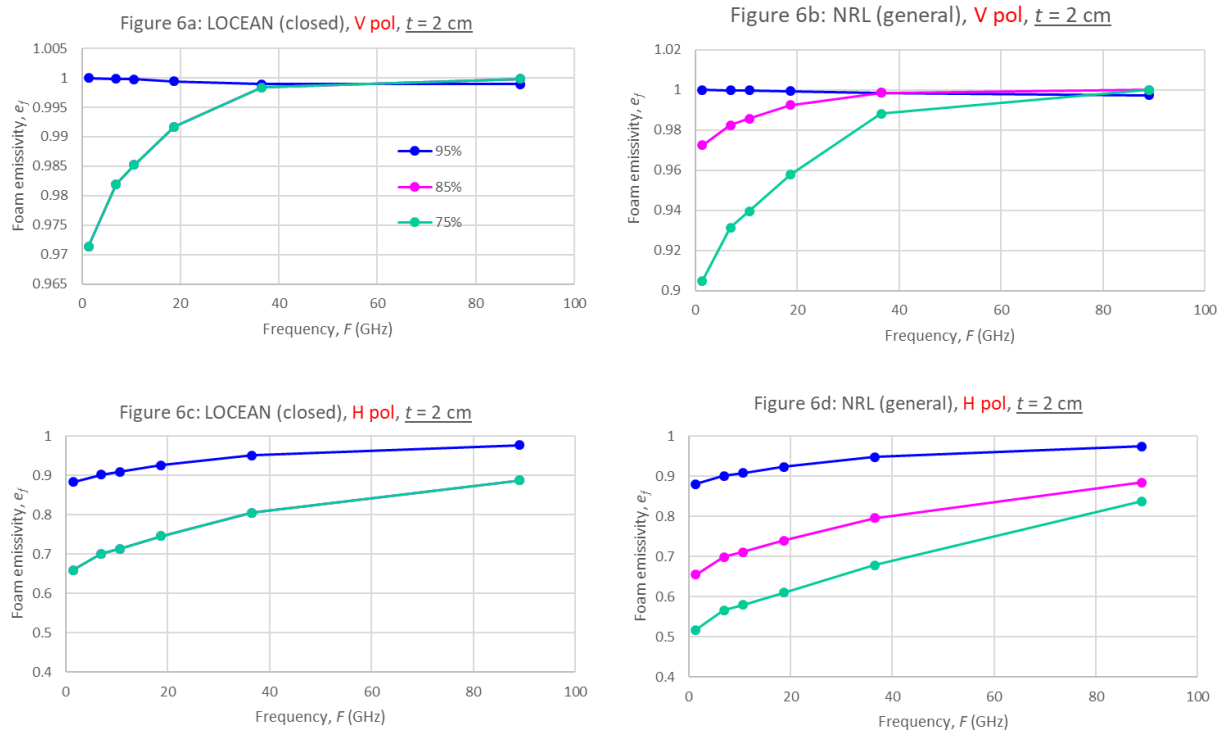

Fig. 6 — Frequency dependence of the foam emissivity e_f from LOCEAN F90 (panels a and c) and NRL IDL (panels b and d) codes for fixed foam thickness layer of 2 cm at different void fraction at the air-foam boundary (color legend): (a) and (b) V pol; (c) and (d) H pol

Figure 6 shows that for both V and H polarizations the general (NRL) formulation of the incoherent approach is more sensitive to variations of v_{af} than the semi-closed form (LOCEAN). Indeed, compare the ever decreasing e_f values in Figure 6b and 6d to often overlapping e_f values in Figure 6a and 6c. Figure 7 quantifies these differences with PDs. For $v_{af} \geq 85\%$, the PDs are below 0.1% for V pol at all frequencies (Figure 7a); for H pol, PD < 1 % (Figure 7b). The PDs are larger at v_{af} = 75%, reaching 7% for V pol at L band and ranging from 17% to 24% for Ka to L bands for H pol.

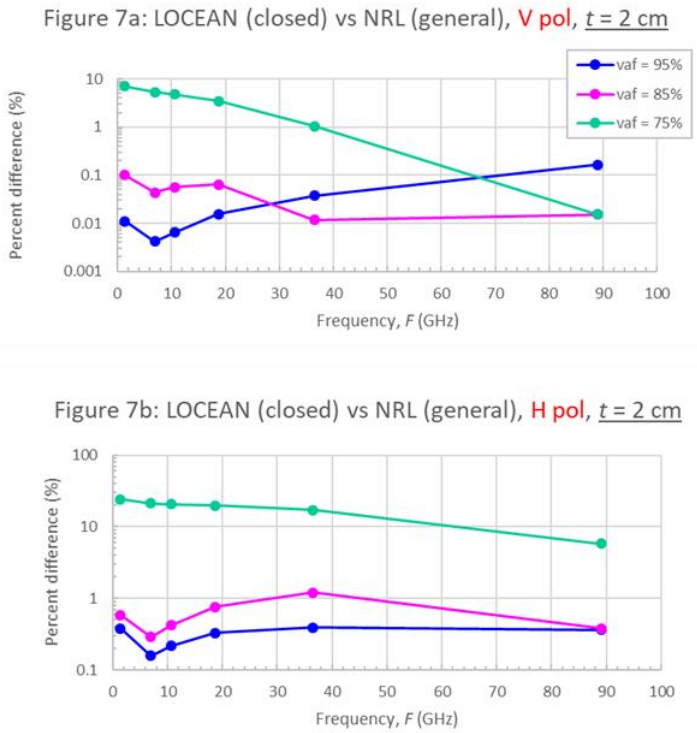

Fig. 7 — Frequency dependence of the percent difference between LOCEAN F90 and NRL IDL codes for fixed foam thickness layer of 2 cm at different void fraction at the air-foam boundary (color legend): (a) V pol; (b) H pol

Variations of the foam layer thickness t (at fixed v_{af} = 95%) do not affect the results of the LOCEAN model. Once again, the NRL model is more sensitive to changes of t. For any t = 1, 2, and 4 cm, the foam emissivity from LOCEAN at both V and H pols changes by less than 10^{-6}. The e_f from the NRL model changes noticeable at higher frequencies (Ka and W band) for t = 4 cm (by 10^{-2}); at lower frequencies and for t = 1 and 2 cm, the e_f values change by 10^{-5}. Figure 8 shows the differences between LOCEAN and NRL for these three *t* values. The PDs are at most around 1% for V pol but mostly below 0.1% (Figure 8a). For H pol, the PD < 1% for 1 and 2 cm thicknesses and is 3% for layers of 4 cm at W band.

6. CONCLUSIONS

There are four main differences between the LOCEAN F90 and NRL IDL implementations of the incoherent approach to modeling foam emissivity e_f (Section 1). The well-known incoherent approach to RT modeling (Appendix A), together with various cases for the reflectivity at various media boundaries (Appendix B), has been used to derive the analytical expressions used for the e_f (Section 3) in F90 and IDL implementations (Section 4). The differences in the F90 and IDL implementations of foam emissivity

calculations have been investigated and reconciled one by one (Table 2) and discrepancies at every step have been quantified (Section 5.1). We also investigate the sensitivity of the two implementations to variations of the observational conditions (section 5.2) and the foam properties (section 5.3).

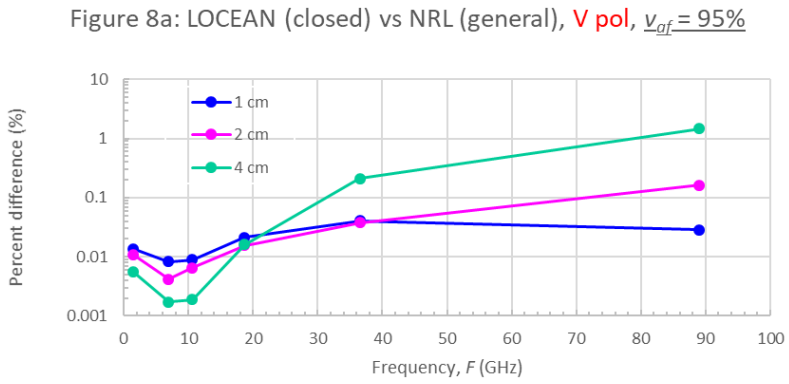

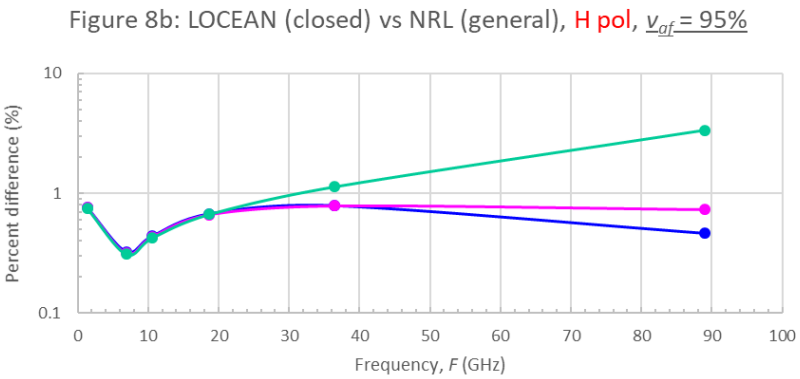

Fig. 8 — Frequency dependence of the percent difference between LOCEAN F90 and NRL IDL codes for fixed void fraction at the air-foam boundary of 95% at different foam layer thicknesses (color legend): (a) V pol; (b) H pol

The conclusions of the comparison of LOCEAN F90 and NRL IDL implementations of the incoherent approach to modeling foam emissivity e_f are as follows:

1) LOCEAN F90 code uses void fraction profile $f_a(z)$ partially, only for the loss factor (14) without integrations (10) and (11). This is tantamount to using the incoherent approach in its semi-closed form (A.33) as compared to its general form given with (7) to (11) and used in the NRL IDL code. The e_f values from the two implementations (Figure 1) differ by less than 1% (Figure 1 and Table 2, green).
2) Use of MW permittivity model produces e_f values from the F90 and IDL implementations differing by at most 1% (Figure 2 and Table 2, magenta). This implies that permittivity models KS77 and S97 perform well even for frequencies well beyond their range of applicability.
3) Fixing an error in the NRL IDL code and correcting the input variables in the LOCEAN F90 code (Appendix C) for the computation of reflectivity Γ_2 at the foam-seawater boundary yields differences in e_f values between the two implementations at most of 1% (Figure 2 and Table 2, yellow).
4) Using consistent integration scheme (namely, the Simpson rule) in both F90 and IDL implementations yields e_f values closest to each other (Figure 3) with differences less than 0.3% (Figure 2 and Table 2, red).

5) Changes in the observational conditions—SST and SSS—yield e_f values from the F90 and IDL implementations differing by less than 0.5% for H pol and even less (0.25%) for V pol (Figures 4 and 5).
6) The general formulation (IDL) of the incoherent approach is more sensitive to changes in the foam properties—upper limit of void fraction profile v_{af} and foam layer thickness t—compared to the semi-closed form (F90) (Figure 6). The differences between the two implementations are less for variations of v_{af} (Figure 7) than for varying foam thicknesses (Figure 8).

Overall, the comparison of LOCEAN and NRL models in two different implementations (F90 and IDL) shows that the semi-closed formulation of the incoherent approach is in most cases a good approximation to the general form. Still, the general formulation shows higher sensitivity to variations of the foam properties and the environmental conditions.

These results and conclusions justify the recommendation to use both implementations for the emissivity of an inhomogeneous foam layer, depending on the study objective. The general formulation [as in (7) to 11)] in slower implementation (as that of the NRL model), but it provides more accurate foam emissivity values. The semi-closed form of the incoherent approach to RTM (A.33) in fast implementation (as that of model LOCEAN) and thus can provide good approximation of foam emissivity values for operational use. The RTM software posted by the ISSI team on the open access site GitHub implements the semi-closed formulation, which provide faster calculations with high quality.

APPENDIX A: REFERENCE CASE FOR INCOHERENT EMISSIVITY

All derivations here follow [4]. We use the derived expressions as a reference to establish differences in formulating foam emissivity e_f in the framework of the incoherent approach to radiative transfer modeling (section 3).

A.1 Thermal emissivity of a homogeneous medium

Attenuation of the electro-magnetic radiation propagating through a medium determines its emissivity. Both absorption and scattering contribute to the attenuation. Coefficients of extinction, absorption, and scattering—k_e, k_a and k_s, respectively—quantify these processes ([4], p. 239):

$$k_e = k_a + k_s \tag{A.1}$$

The single scattering albedo a quantifies the relative contribution of the scattering to the extinction:

$$a = \frac{k_s}{k_e} \tag{A.2}$$

To derive an expression for the emissivity of a medium, let consider a thin horizontal stratum in medium at depth $z = \zeta$ and of thickness $d\zeta$ (Figure A.1). The vertical axis is in oceanographic convention of depth as a positive number with z (or ζ) increasing downwards from the surface (boundary).

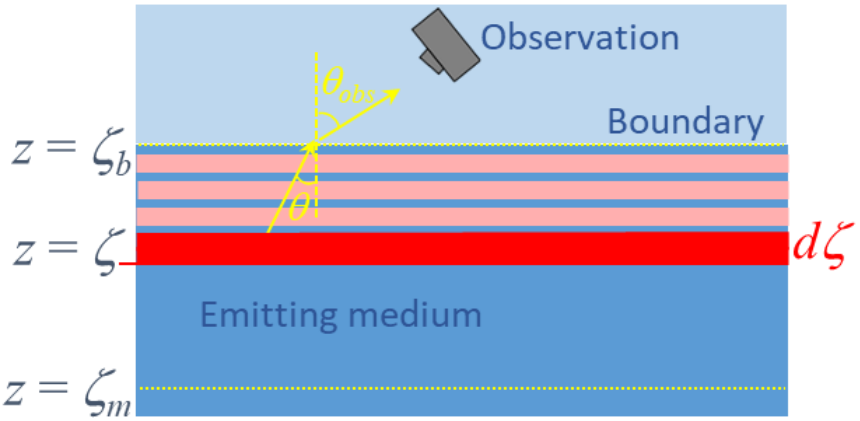

Fig. A.1 — Emission from a stratum at depth $z = \zeta$ with thickness $d\zeta$ (red). The strata above (pink) up to the boundary contribute to the integral attenuation, termed optical depth.

The energy emitted by this stratum in direction θ toward a boundary, in terms of brightness temperature, is:

$$dT_s(\theta, \zeta) = k_a T \sec(\theta) d\zeta \tag{A.3}$$

where k_a is the absorption coefficient of the medium and T is its thermodynamic temperature. For a homogeneous medium, k_a and T are constant.

The strata between this stratum at depth ζ and the boundary at $z = \zeta_b$ attenuate $dT_s(\theta, \zeta)$ while the radiation propagates along a slanted path determined by $\sec(\theta)$ ([4], p. 239; yellow arrow in Fig. A.1). The integrated attenuation of the strata above depth ζ (or below ζ, depending on the boundary position) is termed optical depth (or opacity) $\tau_s(\zeta, \zeta_b)$ of this medium stratum (e.g., [4], Eq. 4.78):

$$\tau_s(\zeta, \zeta_b) = \int_{\zeta}^{\zeta_b} k_a \sec(\theta) d\zeta' = k_a \sec(\theta)(\zeta_b - \zeta) \tag{A.4}$$

where $\zeta < \zeta_b$, as is usually expected for the lower and upper limits of an integral. We note this point because system configuration and/or physical reasoning may suggest the use of inverted integral limits (the lower limit is larger than the upper limit). However, the choice of the integral limits would not affect the result when the integration consistently follows the rule $\int_a^b f(x)dx = -\int_b^a f(x)dx$, where $a < b$. Indeed, following this rule, we will obtain the same result in (A.4) for both choices of integration limits, i.e., $\tau_s(\zeta, \zeta_b) = \tau_s(\zeta_b, \zeta)$. The derivations of the specific emissivity contributions (section A.2.2) will demonstrate this.

To allow for attenuation by both absorption and scattering, we generalize (A.4) by using the medium extinction coefficient k_e instead of k_a:

$$\tau_s(\zeta, \zeta_b) = \int_{\zeta}^{\zeta_b} k_e \sec(\theta) d\zeta' = k_e \sec(\theta)(\zeta_b - \zeta) \tag{A.5}$$

Using (A.3) and (A.5), the energy received close to the boundary from this stratum is:

$$\begin{aligned} dT_s(\theta, \zeta_b) &= dT_s(\theta, \zeta) e^{-\tau_s(\zeta, \zeta_b)} \\ &= k_a T \sec(\theta) \exp[-k_e(\zeta_b - \zeta)\sec(\theta)] d\zeta \end{aligned} \tag{A.6}$$

The exponential term in (A.6) accounts for the losses due to the medium optical depth between ζ and ζ_b. The total energy received at boundary ζ_b from all strata in the medium is then given with the integral of (A.6)

$$\begin{aligned} T_s(\theta, \zeta_b) &= \int_{\zeta_b}^{\zeta_m} dT_s(\theta, \zeta_b) \\ &= \int_{\zeta_b}^{\zeta_m} k_a T \sec(\theta)\, e^{-k_e(\zeta_b - \zeta)\sec(\theta)} d\zeta \end{aligned} \tag{A.7}$$

where $\zeta_m > \zeta_b$ is the stratum depth at a maximum distance from the boundary. We use the general expressions (A.1) to (A.7) to derive the incoherent emissivity expression for a layered system (i.e., a system with more than one boundary).

A.2 Thermal emissivity of a layered system

A.2.1 System configuration

We consider a three-layered system (Figure A.2) with a layer of medium 2 mediating the connection between medium 1 at the layer upper surface ($z = 0$, boundary 1) and medium 3 at the layer bottom surface ($z = t$, boundary 2). The vertical axis is in oceanographic convention of depth (as defined in section A.1). All media are assumed homogenous, each with a specific constant value of permittivity ε_i, thermodynamic temperature T_i, and absorption (or extinction) coefficient k_{ai} (or k_{ei}) where $i = 1, 2, 3$.

Layer 2 emits under angle θ_2 toward both boundary 1 (to provide signal in direction θ_1 in medium 1) and

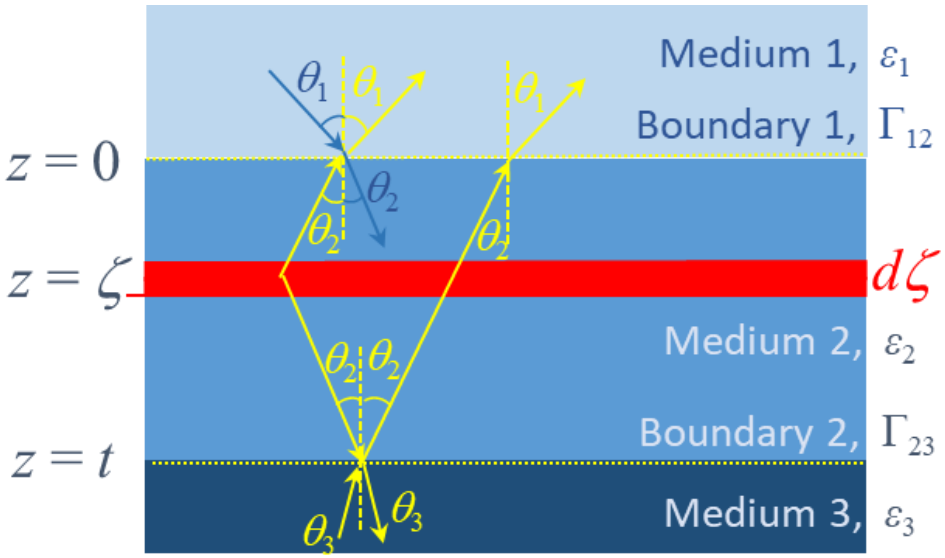

Fig. A.2 — Emission from a stratum at depth $z = \zeta$ with thickness $d\zeta$ (red) in the layer of medium 2. Reflections and refractions occur at boundaries 1 and 2.

boundary 2 (to provide upward reflection in direction θ_2 and transmission into medium 3 in direction θ_3). The self-emission of layer 3 comes toward boundary 2 under angle θ_3, propagating through layer 2 under angle θ_2, and ultimately emitting in medium 1 under angle θ_1. Under the conditions of system homogeneity, all these angles of propagation θ_i ($i = 1, 2, 3$) are of constant values.

A radiometer, observing the three-layered system under angle θ_1, detects brightness temperature signal in dual polarization ($p =$ H and V) $T_B(\theta_1, p)$ that comprises contributions $T_{B2}(\theta_1, p)$ from layer 2 and $T_{B3}(\theta_1, p)$ from medium 3. The radiation from layer 2 consist of upward emission $T_{2U}(\theta_1, p)$ and downward emission $T_{2D}(\theta_1, p)$ (Figure A.2). We thus write ([4], Eqs. 4.150 and 4.151):

$$T_B(\theta_1, p) = T_{B2}(\theta_1, p) + T_{B3}(\theta_1, p) = T_{2U}(\theta_1, p) + T_{2D}(\theta_1, p) + T_{B3}(\theta_1, p) \tag{A.8}$$

Three steps, building on each other, yield the formulation of the net emissivity terms in (A.8). The following sub-sections describe each of these steps. First, using the general formulae A.1 to A.7, we obtain the specific emissivity contributions from media 2 and 3 (section A.2.2). We next modify the specific emissivity contributions to account for their multiple reflections and transmissions at the boundaries (section A.2.3).

Finally, all these elements are put together to obtain the net incoherent emissivity of the layered system comprising all contributions given with the terms in (A.8) (section A.2.4).

A.2.2 Specific emissivity contributions

Upward emission of layer 2

Layer 2 emits upward toward boundary 1 along angle θ_2 (Figure A.2). The boundary depth is $\zeta_b = 0$, the stratum depth at a maximum distance from ζ_b in medium 2 is the layer thickness $\zeta_m = t$ (Figure A.2). Constant values of k_{a2}, k_{e2}, and T_2 describe the layer properties. In these notations, the optical depth for upward propagation (A.5) reads as follows:

$$\tau_{s2}(\zeta, 0) = -\int_{\zeta}^{0} k_{e2}\sec(\theta_2)d\zeta' = -k_{e2}\sec(\theta_2)(0-\zeta) = k_{e2}\zeta\sec(\theta_2) \tag{A.9}$$

Minus sign in the integral is used because in our system configuration the lower integration limit is larger than the upper limit ($\zeta > 0$). From (A.7) and using (A.9), the total energy received at boundary 1 from the layer upward emission is:

$$T_{s2}(\theta_2, 0) = \int_0^t k_{a2}T_2\sec(\theta_2)\, e^{-k_{e2}\zeta\sec(\theta_2)}d\zeta \tag{A.10}$$

Heeding the homogeneity of the layer, multiplying and dividing (A.10) with k_{e2}, and using (A.1) and (A.2) to transform $k_{a2}/k_{e2} = 1 - a_2$, the integration of (A.10) gives the following:

$$\begin{aligned} T_{s2}(\theta_2, 0) &= k_{a2}T_2(1/k_{e2})\int_0^t e^{-k_{e2}\zeta\sec(\theta_2)}d[k_{e2}\zeta\sec(\theta_2)] \\ &= T_2(1-a_2)[-(e^{-\tau_{s2}\cdot t} - e^{-\tau_{s2}\cdot 0})] \\ &= T_2(1-a_2)\left(1 - e^{-k_{e2}\sec(\theta_2)t}\right) \end{aligned} \tag{A.11}$$

Denoting the exponential losses in the entire layer 2 as:

$$\tau_2(0, t) = e^{-k_{e2}\sec(\theta_2)t} \tag{A.12}$$

and defining the loss factor for layer 2 as the inverse of the exponential losses ([4], p. 221):

$$L_2(0, t) \triangleq \frac{1}{\tau_2} = e^{k_{e2}\sec(\theta_2)t} \tag{A.13}$$

we obtain a closed-form expression for the integration of (A.10) ([4], Eq. 4.155):

$$T_{s2}(\theta_2, 0) = T_2(1 - a_2)\left[1 - \frac{1}{L_2}\right] = T_2(1 - a_2)[1 - \tau_2] \quad \text{(A.14)}$$

Downward emission of layer 2

Layer 2 emits downward toward boundary 2 along angle θ_2 (Figure A.2). Because layer 2 radiates isotopically, the total energy received at boundary 2 from the layer downward emission is the same as that for the upward emission (A.14), i.e., $T_{s2}(\theta_2, 0) = T_{s2}(\theta_2, t)$ ([4], p. 242). This is proven here using the general expressions in section A.1.

For the downwelling emission, the boundary depth is $\zeta_b = t$, and the stratum depth at a maximum distance from ζ_b in medium 2 is at boundary 1 with $\zeta_m = 0$ (Figure A.2). The optical depth for downward propagation is:

$$\tau_{s2}(\zeta, t) = \int_{\zeta}^{t} k_{e2} \sec(\theta_2) d\zeta' = k_{e2} \sec(\theta_2)(t - \zeta) \quad \text{(A.15)}$$

Here $\zeta < t$, so no modifications of (A.5) are needed on account of integration limits. The total energy received at boundary 2 from the layer downward emission is:

$$T_{s2}(\theta_2, t) = -\int_{t}^{0} k_{a2} T_2 \sec(\theta_2)\, e^{-k_{e2}\sec(\theta_2)(t-\zeta)} d\zeta \quad \text{(A.16)}$$

Minus sign is used here because $t > 0$. Making the same transformations as for the upward integration and changing $d\zeta$ to $d(t - \zeta)$, the integration of (A.16) gives the following:

$$\begin{aligned} T_{s2}(\theta_2, t) &= -k_{a2} T_2 (1/k_{e2}) \int_{t}^{0} e^{-k_{e2}\sec(\theta_2)(t-\zeta)} d[-k_{e2} \sec(\theta_2)(t - \zeta)] \\ &= T_2(1 - a_2)\left[-\left(e^{-k_{e2}\sec(\theta_2)t} - e^{-k_{e2}\sec(\theta_2).0}\right)\right] \\ &= T_2(1 - a_2)\left(1 - e^{-k_{e2}\sec(\theta_2)t}\right) \end{aligned} \quad \text{(A.17)}$$

Using notations (A.12) and (A.13), we obtain for the integration of (A.16) the same closed form as (A.14):

$$T_{s2}(\theta_2, t) = T_2(1 - a_2)\left[1 - \frac{1}{L_2}\right] = T_2(1 - a_2)[1 - \tau_2] \quad \text{(A.18)}$$

Upward emission of medium 3

The derivation of the contribution of medium 3 follows the same reasoning as for layer 2. Medium 3 emits upward toward boundary 2 along angle θ_3 (Figure A.2). Because medium 3 is semi-infinite, its upward emission is the medium thermodynamic temperature T_3 [4, p. 243]. Here we prove this statement using the general expressions in section A.1 and show that $T_{s3}(\theta_3, t) = T_3$.

For the upward emission from medium 3, the boundary depth is $\zeta_b = t$, and the stratum depth at a maximum distance from ζ_b in medium 3 is $\zeta_m = \infty$ (Figure A.2). Following (A.5), the optical depth for upward propagation is:

$$\tau_{s3}(\zeta, t) = -\int_{\zeta}^{t} k_{a3} \sec(\theta_3) d\zeta' = k_{a3} \sec(\theta_3)(\zeta - t) \tag{A.19}$$

Again, minus sign is used because in the system configuration $\zeta > t$. Only absorption coefficient k_{a3} is used to model a system with no scattering. The total energy received at boundary 2 from upward emission in medium 3 is:

$$T_{s3}(\theta_3, t) = \int_{t}^{\infty} k_{a3} T_3 \sec(\theta_3)\, e^{-k_{a3}\sec(\theta_3)(\zeta - t)} d\zeta \tag{A.20}$$

Changing $d\zeta$ to $d(\zeta - t)$, the integration of (A.20) gives the following:

$$\begin{aligned} T_{s3}(\theta_3, t) &= T_3 \int_{t}^{\infty} e^{-k_{a3}\sec(\theta_3)(\zeta - t)} d[k_{a3}\sec(\theta_3)(\zeta - t)] \\ &= T_3\left[-\left(e^{-k_{a3}\sec(\theta_3).\infty} - e^{-k_{a3}\sec(\theta_3).0}\right)\right] = T_3 \end{aligned} \tag{A.21}$$

A.2.3 Multiple reflections and transmissions

Once at boundary 1, the upward emitted radiation $T_{s2}(\theta_2, 0)$ from layer 2 is a subject to multiple transmissions and reflections from the boundary; both processes are quantified with the reflectivity at boundary 1, Γ_1. The reflected portion of $T_{s2}(\theta_2, 0)$ travels through layer 2, attenuates, and is again transmitted and reflected at boundary 2; this is quantified with the reflectivity Γ_2 of boundary 2. Visualization and quantification of multiple transmissions and reflections of the upward emission are given by [4] in their Figure 4.25a. The effect of these successive processes on $T_{s2}(\theta_2, 0)$ ultimately gives the net upward emission from layer 2, T_{2U}, with a series [4, Eq. 4.158]:

$$T_{2U}(\theta_1, p) = (1 - \Gamma_1) T_{s2}[1 + x + x^2 + x^3 + \cdots] \tag{A.22}$$

where

$$x = \frac{\Gamma_1 \Gamma_2}{L_2^2} = \Gamma_1 \Gamma_2 \tau_2^2 \tag{A.23}$$

For $x^2 < 1$, the series in (A.22) is given by

$$1 + x + x^2 + x^3 + \cdots = (1 - x)^{-1} \tag{A.24}$$

Using (A.23) and (A.24), the closed-form expression for the upward emission from layer 2 is [4, Eq. 4.159]:

$$T_{2U}(\theta_1, p) = \frac{1-\Gamma_1}{1-\Gamma_1\Gamma_2/L_2^2} T_{s2} = \frac{1-\Gamma_1}{1-\Gamma_1\Gamma_2\tau_2^2} T_{s2} \tag{A.25}$$

The downward emission $T_{s2}(\theta_2, t)$ from layer 2 is reflected from boundary 2 (quantified with Γ_2) attenuated while crossing layer 2 on its way upward (quantified with L_2), and then transmitted to medium 1 (quantified with $(1-\Gamma_1)$). These processes are repeated multiple times (Figures 4.25b in [4]) and expressed with series (A.24) [4, Eq. 4.160]:

$$T_{2D}(\theta_1, p) = \frac{\Gamma_2(1-\Gamma_1)}{L_2} T_{s2}[1 + x + x^2 + x^3 + \cdots] \tag{A.26}$$

The net downward emission from layer 2, T_{2D}, is then:

$$T_{2D}(\theta_1, p) = \frac{\Gamma_2(1-\Gamma_1)}{L_2(1-\Gamma_1\Gamma_2/L_2^2)} T_{s2} \tag{A.27}$$

Transmissions $(1-\Gamma_2)$ at boundary 2 and $(1-\Gamma_1)$ at boundary 1, together with attenuation L_2 while crossing layer 2, deliver the upward emission $T_{s3}(\theta_3, t)$ of medium 3 to medium 1. Subsequent multiple reflections and transmissions are accounted for again with term $1/(1-\Gamma_1\Gamma_2/L_2^2)$. The net upward emission from medium 3 is thus given as [4, Eq. 4.162]:

$$T_{B3}(\theta_1, p) = \frac{(1-\Gamma_1)(1-\Gamma_2)}{L_2(1-\Gamma_1\Gamma_2/L_2^2)} T_{s3} \tag{A.28}$$

We now have formulated the three terms $T_{2U}(\theta_1, p)$, $T_{2D}(\theta_1, p)$, and $T_{B3}(\theta_1, p)$ in (A.8).

A.2.4 Net incoherent emissivity of homogeneous layered system

Adding (A.25) and (A.27), we obtain the emissivity contribution from layer 2 [4, Eq. 4.161]:

$$T_{B2}(\theta_1, p) = T_{2U}(\theta_1, p) + T_{2D}(\theta_1, p) = \frac{(1-\Gamma_1)\left(1+\frac{\Gamma_2}{L_2}\right)}{1-\Gamma_1\Gamma_2/L_2^2} T_{s2} \tag{A.29}$$

Next, we obtain the total signal from the media 2 and 3 in medium 1 by adding (A.28) and (A.29) [4, Eq. 4.163:

$$T_B(\theta_1, p) = T_{B2}(\theta_1, p) + T_{B3}(\theta_1, p) = \frac{1-\Gamma_1}{1-\Gamma_1\Gamma_2/L_2^2}\left[\left(1+\frac{\Gamma_2}{L_2}\right) T_{s2} + \frac{1-\Gamma_2}{L_2} T_{s3}\right] \tag{A.30}$$

Plugging in (A.30) the closed form solutions (A.14) for T_{s2} and (A.21) for T_{s3}, we receive the full expression for the brightness temperature in medium 1 emanated from media 2 and 3 [4, Eq. 4.163]:

$$T_B(\theta_1,p) = \frac{1-\Gamma_1}{1-\Gamma_1\Gamma_2/L_2^2}\left[\left(1+\frac{\Gamma_2}{L_2}\right)\left(1-\frac{1}{L_2}\right)(1-a_2)T_2 + \frac{1-\Gamma_2}{L_2}T_3\right] \quad \text{(A.31)}$$

Assuming that media 2 and 3 have the same thermodynamic temperatures $T_2 = T_3 = T$, the radiometric signal from the emitting layered system is:

$$T_B(\theta_1,p) = \frac{1-\Gamma_1}{1-\Gamma_1\Gamma_2/L_2^2}\left[\left(1+\frac{\Gamma_2}{L_2}\right)\left(1-\frac{1}{L_2}\right)(1-a_2) + \frac{1-\Gamma_2}{L_2}\right]T \quad \text{(A.32)}$$

By virtue of brightness temperature definition (the product of the medium emissivity e and its thermodynamic temperature, $T_B = eT$), we have from (A.32) the closed form of the incoherent emissivity of the system [4, Eq. 4.166]:

$$e_i(\theta_1,p) = \frac{1-\Gamma_1}{1-\Gamma_1\Gamma_2/L_2^2}\left[\left(1+\frac{\Gamma_2}{L_2}\right)\left(1-\frac{1}{L_2}\right)(1-a_2) + \frac{1-\Gamma_2}{L_2}\right] \quad \text{(A.33)}$$

If the scattering in layer 2 is negligible, i.e., $a_2 \approx 0$, the form for the incoherent emissivity is simplified [18, 1986, Eq. 18.41]:

$$e_i(\theta_1,p) = \frac{1-\Gamma_1}{1-\Gamma_1\Gamma_2/L_2^2}(1-\Gamma_2/L_2^2) \quad \text{(A.34a)}$$

$$= \frac{1-\Gamma_1}{1-\Gamma_1\Gamma_2\tau_2^2}(1-\Gamma_2\tau_2^2) \quad \text{(A.34b)}$$

Form (A.33) is useful for computations of a variety of media because it allows to model non-scattering media by setting $a_2 = 0$, yet leaves the possibility of considering scattering media when $a_2 \neq 0$.

APPENDIX B: REFERENCE CASE FOR FRESNEL REFLECTIVITY

The closed form for incoherent emissivity of a layered system (Appendix A) contains the reflectivity of boundaries 1 (Γ_1) and 2 (Γ_2). In layered systems comprising different media (Figure A.2), the formulations of Γ_1 and Γ_2 differ due to differing permittivity properties ε_i ($i = 1, 2, 3$). Here, we derive the forms of Γ_1 and Γ_2 following [4, Chapter 4-11.2]. We use these formulations as a reference to compare their implementations (section 4).

Note that Γ_1 and Γ_2 used in the incoherent emissivity expression (A.33) refer to each boundary (1 or 2), while the notations in the derivation below refer to the media on each side of the boundary. That is, the reflectivity at boundary 1 between media 1 and 2 is denotes as $\Gamma_1 \equiv \Gamma_{1,2}$ and the reflectivity at boundary 2 between media 2 and 3 is denoted as $\Gamma_2 \equiv \Gamma_{2,3}$ (Figure A.2). In the media-related notation (versus boundary-related notation), the order of the subscripts shows the direction of propagation toward the boundary: i.e.,

$\Gamma_{1,2}$ denotes radiation propagating from medium 1 towards medium 2, while $\Gamma_{2,1}$ denotes propagation from medium 2 towards medium 1 (more on this is given in section B.2).

B.1 Basic formulae

Consider radiation propagating from medium 1 towards medium 2 under angle θ_1 (Figure B.1).

The Fresnel reflection coefficient $r_{1,2}$, obtained from the normalized (relative) impedances Z_i of the media, determines the reflectivity at the interface between them [4, Eq. 4.120]:

$$\Gamma_{1,2}(\theta_1, p) = \left|r_{1,2}(\theta_1, p)\right|^2 = \left|\frac{\mathrm{Z}_2 - \mathrm{Z}_1}{\mathrm{Z}_2 + \mathrm{Z}_1}\right|^2 \tag{B.1}$$

where $p = \mathrm{H}, \mathrm{V}$ is the radiation polarization and the impedances are [4, Eq. 4.121]:

$$\mathrm{Z}_i = \begin{cases} \eta_i \cos\theta_i \ , \ p = \mathrm{V} \\ \eta_i \sec\theta_i \ , \ p = \mathrm{H} \end{cases} \tag{B.2}$$

with $i = 1, 2$, $\sec\vartheta_i = 1/\cos\vartheta_i$, and [4, Eq. 4.115]:

$$\eta_i = \sqrt{\frac{\mu_i}{\varepsilon_i}} = \frac{1}{\sqrt{\varepsilon_i}} = \frac{1}{n_i} \tag{B.3}$$

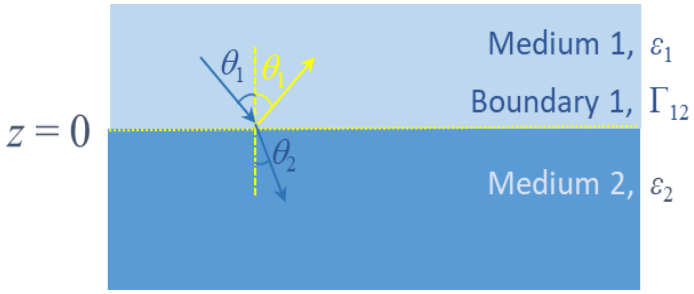

Fig. B.1 — Derivation of the Fresnel reflectivity at the boundary of two media.

In (B.3), the media permeabilities are $\mu_i = 1$ for microwave frequencies, and the media permittivities ε_i give the refraction indeces $n_i = \sqrt{\varepsilon_i}$. The reflected angle in medium 1 is equal to the incident angle θ_1, while the refracted angle in medium 2, θ_2, is related to θ_1 via the Snell law [4, Eq. 2.51]:

$$n_2 \sin\theta_2 = n_1 \sin\theta_1 \tag{B.4a}$$

$$\sqrt{\varepsilon_2}\sin\theta_2 = \sqrt{\varepsilon_1}\sin\theta_1 \tag{B.4b}$$

The Snell law yields representation of the refractive angle in terms of the incident angle:

$$\sin\theta_2 = \sqrt{\frac{\varepsilon_1}{\varepsilon_2}}\sin\theta_1 \tag{B.5a}$$

$$\cos\theta_2 = \frac{1}{\sqrt{\varepsilon_2}}\sqrt{\varepsilon_2 - \varepsilon_1 \sin^2\theta_1} \tag{B.5b}$$

Using (B.5b) in (B.2) and (B.1), the Fresnel reflection coefficients for H and V are:

$$r_{1,2}(\theta_1, \mathrm{V}) = \left|\frac{\varepsilon_2\cos\theta_1 - \sqrt{\varepsilon_1}\sqrt{\varepsilon_2 - \varepsilon_1\sin^2\theta_1}}{\varepsilon_2\cos\theta_1 + \sqrt{\varepsilon_1}\sqrt{\varepsilon_2 - \varepsilon_1\sin^2\theta_1}}\right| = \left|\frac{\varepsilon_2\cos\theta_1 - \sqrt{\varepsilon_1\varepsilon_2 - \varepsilon_1^2\sin^2\theta_1}}{\varepsilon_2\cos\theta_1 + \sqrt{\varepsilon_1\varepsilon_2 - \varepsilon_1^2\sin^2\theta_1}}\right| \tag{B.6a}$$

$$r_{1,2}(\theta_1, \mathrm{H}) = \left|\frac{\sqrt{\varepsilon_1}\cos\theta_1 - \sqrt{\varepsilon_2 - \varepsilon_1\sin^2\theta_1}}{\sqrt{\varepsilon_1}\cos\theta_1 + \sqrt{\varepsilon_2 - \varepsilon_1\sin^2\theta_1}}\right| \tag{B.6b}$$

It can be shown that for the inverse case—when the radiation propagates from medium 2 towards medium 1 under incident angle θ_2— we have [4, Eq. 4.123]:

$$r_{2,1}(\theta_2, p) = (-1)^s\left(\frac{\mathrm{Z}_1 - \mathrm{Z}_2}{\mathrm{Z}_1 + \mathrm{Z}_2}\right) = -r_{1,2}(\theta_1, p) \qquad s = \begin{cases} 0 & \text{for } p = \mathrm{H} \\ 1 & \text{for } p = \mathrm{V} \end{cases} \tag{B.7a}$$

i.e., from (B.1) we have

$$\Gamma_{2,1}(\theta_2, p) = \Gamma_{1,2}(\theta_1, p) \tag{B.7b}$$

B.2 Fresnel coefficients for a layered system

For a layered system such as in Figure A.2, (B.6) gives the Fresnel coefficients at boundary 1 for radiation propagating from media 1 toward medium 2 under incident angle θ_1.

We can easily obtain the Fresnel reflectivity at boundary 2 for radiation propagating from media 2 toward medium 3 under incident angle θ_2 using the following substitutions: $\varepsilon_1 \equiv \varepsilon_2$, $\varepsilon_2 \equiv \varepsilon_3$, and $\theta_1 \equiv \theta_2$. The Fresnel reflectivity for H and V polarizations at boundary 2 between media 2 and 3 is:

$$r_{2,3}(\theta_2, \mathrm{V}) = \left|\frac{\varepsilon_3\cos\theta_2 - \sqrt{\varepsilon_2}\sqrt{\varepsilon_3 - \varepsilon_2\sin^2\theta_2}}{\varepsilon_3\cos\theta_2 + \sqrt{\varepsilon_2}\sqrt{\varepsilon_3 - \varepsilon_2\sin^2\theta_2}}\right| \tag{B.8a}$$

$$r_{2,3}(\theta_2, \mathrm{H}) = \left|\frac{\sqrt{\varepsilon_2}\cos\theta_2 - \sqrt{\varepsilon_3 - \varepsilon_2\sin^2\theta_2}}{\sqrt{\varepsilon_2}\cos\theta_2 + \sqrt{\varepsilon_3 - \varepsilon_2\sin^2\theta_2}}\right| \tag{B.8b}$$

Rigorous derivation of $r_{2,3}(\theta_2, p)$ using (B.1) to (B.5) [instead of substituting subscripts in (B.6)] yields the same result as in (B.8).

For the case of homogeneous layer, the refractive angle θ_2 in (B.8) remains constant through the layer from boundary 1 to boundary 2 (Figure A.2). Therefore, we can use (B.5) in (B.8) to represent θ_2 with the incident angle θ_1 from medium 1. Then the Fresnel reflectivity at boundary 2 in terms of θ_1 is:

$$r_{2,3}(\theta_1, \mathrm{V}) = \left| \frac{\varepsilon_2\sqrt{\varepsilon_3 - \varepsilon_1 \sin^2\theta_1} - \varepsilon_3\sqrt{\varepsilon_2 - \varepsilon_1 \sin^2\theta_1}}{\varepsilon_2\sqrt{\varepsilon_3 - \varepsilon_1 \sin^2\theta_1} + \varepsilon_3\sqrt{\varepsilon_2 - \varepsilon_1 \sin^2\theta_1}} \right| \tag{B.9a}$$

$$r_{2,3}(\theta_1, \mathrm{H}) = \left| \frac{\sqrt{\varepsilon_2 - \varepsilon_1 \sin^2\theta_1} - \sqrt{\varepsilon_3 - \varepsilon_1 \sin^2\theta_1}}{\sqrt{\varepsilon_2 - \varepsilon_1 \sin^2\theta_1} + \sqrt{\varepsilon_3 - \varepsilon_1 \sin^2\theta_1}} \right| \tag{B.9b}$$

We can generalize (B.6) and (B.8) to represent the reflectivity between any media k and l ($k < l$) for radiation propagating from medium k towards medium l under incident angle θ_k as follows:

$$r_{k,l}(\theta_k, \mathrm{V}) = \left| \frac{\varepsilon_l \cos\theta_k - \sqrt{\varepsilon_k}\sqrt{\varepsilon_l - \varepsilon_k \sin^2\theta_k}}{\varepsilon_l \cos\theta_k + \sqrt{\varepsilon_k}\sqrt{\varepsilon_l - \varepsilon_k \sin^2\theta_k}} \right| \tag{B.10a}$$

$$r_{k,l}(\theta_k, \mathrm{H}) = \left| \frac{\sqrt{\varepsilon_k}\cos\theta_k - \sqrt{\varepsilon_l - \varepsilon_k \sin^2\theta_k}}{\sqrt{\varepsilon_k}\cos\theta_k + \sqrt{\varepsilon_l - \varepsilon_k \sin^2\theta_k}} \right| \tag{B.10b}$$

From (B.7), the following is valid for the inverse configuration (radiation incident on the boundary from medium l towards medium k under angle θ_l):

$$\Gamma_{l,k}(\theta_l, p) = \Gamma_{k,l}(\theta_k, p) \tag{B.10c}$$

We use the general expressions (B.6), (B.8), and (B.9) to represent the Fresnel reflection coefficients for specific combinations of media.

B.3 Fresnel reflection coefficients for specific media combinations

B.3.1 Air-seawater boundary

Reflection at the air-seawater interface is the most common remote sensing object of observation. For this case, Figure B.1 is applicable with permittivity of air $\varepsilon_1 = 1$ and of seawater $\varepsilon_2 \equiv \varepsilon$. From (B.6), the Fresnel coefficients for H and V polarizations are thus as follows:

$$r_{1,2}(\theta_1, \mathrm{V}) = \left| \frac{\varepsilon\cos\theta_1 - \sqrt{\varepsilon - \sin^2\theta_1}}{\varepsilon\cos\theta_1 + \sqrt{\varepsilon - \sin^2\theta_1}} \right| \tag{B.11a}$$

$$r_{1,2}(\theta_1, \mathrm{H}) = \left| \frac{\cos\theta_1 - \sqrt{\varepsilon - \sin^2\theta_1}}{\cos\theta_1 + \sqrt{\varepsilon - \sin^2\theta_1}} \right| \tag{B.11b}$$

B.3.2 A system with homogeneous layer

Figure A.2 represent a system for this case with medium 2 being a homogeneous layer with $\varepsilon_2 = \mathrm{const}$ interfaced on top with air ($\varepsilon_1 = 1$) and on bottom with seawater $\varepsilon_3 \equiv \varepsilon$. Using these notations, the general expressions (section B.2) provide specific forms for the Fresnel reflectivity at the layer boundaries.

Boundary 1: air and medium 2

For boundary 1, we use (B.6) and have the Fresnel reflectivity for H and V polarizations as follows (compare to (4.132) for Fig. 4.19 in [4]):

$$r_{1,2}(\theta_1, \mathrm{V}) = \left| \frac{\varepsilon_2 \cos\theta_1 - \sqrt{\varepsilon_2 - \sin^2\theta_1}}{\varepsilon_2 \cos\theta_1 + \sqrt{\varepsilon_2 - \sin^2\theta_1}} \right| \tag{B.12a}$$

$$r_{1,2}(\theta_1, \mathrm{H}) = \left| \frac{\cos\theta_1 - \sqrt{\varepsilon_2 - \sin^2\theta_1}}{\cos\theta_1 + \sqrt{\varepsilon_2 - \sin^2\theta_1}} \right| \tag{B.12b}$$

Boundary 2: medium 2 and seawater

For boundary 2, we use (B.8) and have the Fresnel reflectivity for H and V polarizations as follows:

$$r_{2,3}(\theta_2, \mathrm{V}) = \left| \frac{\varepsilon \cos\theta_2 - \sqrt{\varepsilon_2}\sqrt{\varepsilon - \varepsilon_2 \sin^2\theta_2}}{\varepsilon \cos\theta_2 + \sqrt{\varepsilon_2}\sqrt{\varepsilon - \varepsilon_2 \sin^2\theta_2}} \right| \tag{B.13a}$$

$$r_{2,3}(\theta_2, \mathrm{H}) = \left| \frac{\sqrt{\varepsilon_2}\cos\theta_2 - \sqrt{\varepsilon - \varepsilon_2 \sin^2\theta_2}}{\sqrt{\varepsilon_2}\cos\theta_2 + \sqrt{\varepsilon - \varepsilon_2 \sin^2\theta_2}} \right| \tag{B.13b}$$

Boundary 2: medium 2 and seawater via incident angle in air

For boundary 2 in terms of incidence angle θ_1 we use (B.9) and have the Fresnel reflectivity for H and V polarizations as follows:

$$r_{2,3}(\theta_1, \mathrm{V}) = \left| \frac{\varepsilon_2 \sqrt{\varepsilon - \sin^2\theta_1} - \varepsilon\sqrt{\varepsilon_2 - \sin^2\theta_1}}{\varepsilon_2 \sqrt{\varepsilon - \sin^2\theta_1} + \varepsilon\sqrt{\varepsilon_2 - \sin^2\theta_1}} \right| \tag{B.14a}$$

$$r_{2,3}(\theta_1, \mathrm{H}) = \left| \frac{\sqrt{\varepsilon_2 - \sin^2\theta_1} - \sqrt{\varepsilon - \sin^2\theta_1}}{\sqrt{\varepsilon_2 - \sin^2\theta_1} + \sqrt{\varepsilon - \sin^2\theta_1}} \right| \tag{B.14b}$$

APPENDIX C: MODIFICATIONS OF F90 CODE FOR Γ_2 COMPUTATION

The subroutine and variables mentioned in this appendix can be found in the PARMIO F90 code in GitHub. To use correct input variables for the calculations of the reflectivity Γ_2 at the foam-seawater boundary in the F90 code, we made changes in some subroutines in module 'mod_foam_emiss.f90'.

C.1 Changes in Subroutine 'esf_anguelova'

Add to INTERNAL declarations: REAL (KIND=8) :: tfw

Add calculations of $\theta_f\big|_{z=t}$ with function 'thetaz' as follows:

! Refractive angle at the foam-seawater boundary z = t

tfw=thetaz(t,t,thetai,vaf,vfw,m,hz,sigw_re,sigw_im)

tfw=tfw*180/pi

Comment out the original call to subroutine 'IncohEmissivity_TwoLayer' and change it to a new call as follows:

! New version because we need seawater permittivity epsi

! and refractive angle at the foam-water boundary tfw

CALL IncohEmissivity_TwoLayer(epsi, sigfoam1,sigfoam2, thetai, tfw, aa, taof,evfoam, ehfoam)

C.2 Changes in Subroutine 'IncohEmissivity_TwoLayer'

Comment out the original subroutine name and list of inputs and outputs in order to define the subroutine with more inputs as follows:

! Original

!SUBROUTINE IncohEmissivity_TwoLayer(eps2,eps3,theta_i,a, kappa_e,e_v_inc,e_h_inc)

! Now changed to get 2 more input variables: epsw and theta2

SUBROUTINE IncohEmissivity_TwoLayer(epsw,eps2,eps3,theta_i,theta2, a, kappa_e,e_v_inc,e_h_inc)

Declare additional variable: COMPLEX (KIND=8) epsw

Comment out the calculations of: thetha1, n1, n2, and theta2

Comment out the original call to subroutine 'ReflTransm_PlanarBoundary' and code new call as follows:

! 23 interface

! This is the original call for Gamma2.

! For correct calculation of Gamma 2, the input variables eps2, eps3, and thetha2 should be different

!CALL ReflTransm_PlanarBoundary(eps2, eps3, theta2, rhoh, rhov,gammah23, gammav23, tauh, tauv, Th, Tv);

! Here is the call with correct input variables

CALL ReflTransm_PlanarBoundary(eps3, epsw, theta2, rhoh, rhov,gammah23, gammav23, tauh, tauv, Th, Tv);

ACKNOWLEDGEMENT

The author, M. D. Anguelova, acknowledges Dr. Michael H. Bettenhausen for his consultations on the Fortran code and useful discussions on the physics of the roughness and foam models.

REFERENCES

1 S. English, C. Prigent, B. Johnson, S. Yueh, E. Dinnat, J. Boutin, S. Newman, M. Anguelova, T. Meissner, M. Kazumori, F. Weng, A. Supply, L. Kilic, M. Bettenhausen, A. Stoffelen, and C. Accadia, 2020, "Reference-Quality Emission and Backscatter Modeling for the Ocean," Bull. Amer Meteor. Soc., 101(10), E1593-E1601. doi:10.1175/BAMS-D-20-0085.1

2 M.D. Anguelova, E. Dinnat, L. Kilic, M.H. Bettenhausen, S. English, C. Prigent, T. Meissner, J. Boutin, S. Newman, B. Johnson, S. Yueh, M. Kazumori, F. Weng, A. Stoffelen, C. Accadia, "Foam emissivity modelling with foam properties tuned by frequency and polarization," Proceedings of the International Geoscience and Remote Sensing Symposium (IGARSS), Kuala Lumpur, Malaysia, 2022, pp. 6923–6926. doi: 10.1109/IGARSS46834.2022.9883610.

3 E. Dinnat, S. English, C. Prigent, L. Kilic, M. Anguelova, S. Newman, T. Meissner, J. Boutin, M. Bettenhausen, A. Stoffelen, S. Yueh, B. Johnson, F. Weng, M. Kazumori, C. Accadia, "PARMIO: A reference quality model for ocean surface emissivity and backscatter from the microwave to the infrared," Proceedings of the International Geoscience and Remote Sensing Symposium (IGARSS), Pasadena, California, USA, 2023, submitted.

4 F. Ulaby, R. Moore, and A. Fung, *Microwave remote sensing: Active and passive, Vol. I* (Addison-Wesley Publishing Company, Reading, Massachusetts, USA, 1981).

5 M.D. Anguelova, and P.W. Gaiser, 2013, "Microwave emissivity of sea foam layers with vertically inhomogeneous dielectric properties," Remote Sensing of Environment, 139, 81–96. doi:10.1016/j.rse.2013.07.017

6 M.D. Anguelova, P.W. Gaiser, 2012, "Dielectric and radiative properties of sea foam at microwave requencies: Conceptual understanding of foam emissivity," Remote Sensing, 4(5), 1162–1189. doi:10.3390/rs4051162

7 X. Yin, J. Boutin, E. Dinnat, Q. Song, A. Martin, 2016, "Roughness and foam signature on SMOS-MIRAS brightness temperatures: A semi-theoretical approach," Remote sensing of environment, 180, 221–233. doi: 10.1016/j.rse.2016.02.005

8 L. Kilic, C. Prigent, J. Boutin, T. Meissner, S. English, S. Yueh, 2019, "Comparisons of ocean radiative transfer models with SMAP and AMSR2 observations," Journal of Geophysical Research: Oceans, 124, 7683–7699. doi:10.1029/2019JC015493

9 L. Klein, C. Swift, 1977, "An improved model for the dielectric constant of sea water at microwave frequencies," IEEE Journal of Oceanic Engineering, 2(1), 104–111. doi: 10.1109/JOE.1977.1145319

10 A.P. Stogryn, *Equations for the permittivity of sea water. Technical Report* (GenCorp Aerojet, Azusa, California, USA, 1997).

11 T. Meissner, and F.J. Wentz, 2004, "The complex dielectric constant of pure and sea water from microwave satellite observations," IEEE Trans. Geosci. Remote Sens., 42(9), 1836–1849. doi: 10.1109/TGRS.2004.831888

12 T. Meissner, F.J. Wentz, 2012, "The emissivity of the ocean surface between 6 and 90 GHz over a large range of wind speeds and Earth incidence angle," Transactions on Geoscience and Remote Sensing, 50(8), 3004–3026. doi:10.1109/TGRS.2011.2179662

13 M.D. Anguelova, 2008, "Complex dielectric constant of sea foam at microwave frequencies," Journal of Geophysical Research, 113, C08001. doi:10.1029/2007JC004212.

14 M.D. Anguelova, "Absorption and scattering by sea foam streaks at millimeter-wave frequencies," Proceedings of the International Geoscience and Remote Sensing Symposium (IGARSS), 2020, pp. 5662-5665, doi**:**10.1109/IGARSS39084.2020.9323127.

15 M.D. Anguelova, P.W. Gaiser, 2011, "Skin depth at microwave frequencies of sea foam layers with vertical profile of void fraction," Journal of Geophysical Research, 116, C11002. doi:10.1029/2011JC007372

16 T. Meissner, 2020, 3rd ISSI meeting (virtual), https://www.issibern.ch/teams/oceansurfemiss/wp-content/uploads/2021/01/Meissner_ISSI_Team_Meeting_Dec_2020_Dielectric.pdf

17 W. Drenckhan, S. Hutzler, 2015, "Structure and energy of liquid foams," Advances in Colloid and Interface Science, 224, 1–16. doi:10.1016/j.cis.2015.05.004

18 F. Ulaby, R. Moore, A. Fung, *Microwave remote sensing: Active and passive, Vol. III* (Artech House, Inc., Dedham, Massachusetts, USA, 1986).